

DATING PROTEROZOIC FAULT MOVEMENT  
USING K-Ar GEOCHRONOLOGY OF ILLITE  
SEPARATED FROM LITHIFIED FAULT GOUGE

by  
HN Cutten, H Zwingmann, T Uysal, A Todd  
and SP Johnson





Government of **Western Australia**  
Department of **Mines, Industry Regulation  
and Safety**

REPORT 214

# DATING PROTEROZOIC FAULT MOVEMENT USING K–Ar GEOCHRONOLOGY OF ILLITE SEPARATED FROM LITHIFIED FAULT GOUGE

by

HN Cutten, H Zwingmann<sup>1</sup>, T Uysal<sup>2</sup>, A Todd<sup>2</sup> and SP Johnson

<sup>1</sup> Department of Geology and Mineralogy, Kitashirakawa Oiwakecho, Sakyo-ku, Kyoto University, Kyoto, 606–8502, Japan

<sup>2</sup> CSIRO Australian Resources Research Centre (ARRC), Kensington, Perth WA 6155, Australia

PERTH 2021



**Geological Survey of  
Western Australia**

**MINISTER FOR MINES AND PETROLEUM**  
**Hon Bill Johnston MLA**

**DIRECTOR GENERAL, DEPARTMENT OF MINES, INDUSTRY REGULATION AND SAFETY**  
**David Smith**

**EXECUTIVE DIRECTOR, GEOLOGICAL SURVEY AND RESOURCE STRATEGY**  
**Jeff Haworth**

#### **REFERENCE**

**The recommended reference for this publication is:**

Cutten, HN, Zwingmann, H, Uysal, T, Todd, A and Johnson, SP 2021, Dating Proterozoic fault movement using K–Ar geochronology of illite separated from lithified fault gouge: Geological Survey of Western Australia, Report 214, 25p.

**ISBN** 978-1-74168-918-1

**ISSN** 1834-2280



A catalogue record for this book is available from the National Library of Australia

Grid references in this publication refer to the Geocentric Datum of Australia 1994 (GDA94). Locations mentioned in the text are referenced using Map Grid Australia (MGA) coordinates, Zone 50. All locations are quoted to at least the nearest 100 m.

#### **Disclaimer**

This product uses information from various sources. The Department of Mines, Industry Regulation and Safety (DMIRS) and the State cannot guarantee the accuracy, currency or completeness of the information. Neither the department nor the State of Western Australia nor any employee or agent of the department shall be responsible or liable for any loss, damage or injury arising from the use of or reliance on any information, data or advice (including incomplete, out of date, incorrect, inaccurate or misleading information, data or advice) expressed or implied in, or coming from, this publication or incorporated into it by reference, by any person whatsoever.

#### **Published 2021 by the Geological Survey of Western Australia**

This Report is published in digital format (PDF) and is available online at <[www.dmir.s.wa.gov.au/GSWApublications](http://www.dmir.s.wa.gov.au/GSWApublications)>.



© State of Western Australia (Department of Mines, Industry Regulation and Safety) 2021

With the exception of the Western Australian Coat of Arms and other logos, and where otherwise noted, these data are provided under a Creative Commons Attribution 4.0 International Licence. (<http://creativecommons.org/licenses/by/4.0/legalcode>)

#### **Further details of geoscience publications are available from:**

Information Centre  
Department of Mines, Industry Regulation and Safety  
100 Plain Street  
EAST PERTH WESTERN AUSTRALIA 6004  
Telephone: +61 8 9222 3459 Email: [publications@dmirs.wa.gov.au](mailto:publications@dmirs.wa.gov.au)  
[www.dmir.s.wa.gov.au/GSWApublications](http://www.dmir.s.wa.gov.au/GSWApublications)

**Cover image:** An exposure of the South Brumby Creek Fault (Mount Vernon Fault system), showing 20 cm reverse offset of alternating beds of sandstone and siltstone of the Kiangi Creek Formation. Fault gouge from the fault has been K–Ar dated at  $1141.2 \pm 58.6$  Ma indicating displacement during the Mutherbukin Tectonic Event

## Contents

Abstract .....	1
Introduction .....	1
Geological setting .....	2
Timing of reactivation events in basement rocks of the Gascoyne Province .....	3
Mutherbukin Tectonic Event .....	3
Edmundian Orogeny .....	7
Kuparr Tectonic Event .....	7
Mulka Tectonic Event .....	7
Sample collection .....	7
Mount Vernon Fault system .....	7
Quartzite Well Fault system .....	9
Analytical methods .....	10
Sample processing .....	10
Petrography .....	10
Scanning electron microscopy .....	10
Transmission electron microscopy .....	10
X-ray diffraction .....	10
K–Ar dating .....	10
Illite polytypes .....	10
Illite crystallinity .....	13
Results .....	13
Petrography .....	13
Scanning electron microscopy (SEM) .....	16
Transmission electron microscopy (TEM) .....	16
X-ray diffraction .....	17
Illite crystallinity .....	17
K–Ar dating .....	17
Mount Vernon Fault system .....	19
Quartzite Well Fault system .....	19
Discussion .....	20
Kuparr Tectonic Event .....	20
Neoproterozoic and Phanerozoic dates .....	22
Conclusions .....	22
Acknowledgements .....	23
References .....	23

## Figures

1. Location of the Edmund and Collier Basins in the Capricorn Orogen .....	2
2. Stratigraphy of the Edmund and Collier Groups showing subdivision into depositional packages and formations .....	4
3. Locations of dated K–Ar samples from the Mount Vernon and Quartzite Well Fault systems .....	5
4. Surface expressions of faulting in the Edmund and Collier Groups .....	8
5. Abra drillcore showing lithified fault gouge sampled for K–Ar dating .....	9
6. Illite Age Analysis (IAA) and determination of clay polytypes for GSWA 189281 .....	12
7. Illite crystallinity (Kübler Index, KI) classification .....	13
8. Thin section petrography of fault rocks .....	14
9. SEM and TEM images of representative samples .....	15
10. Ages for tectonic events, based on published U–Pb, Ar/Ar, Rb–Sr dates, and K–Ar dates in this study .....	16

## Tables

1. Published dates and events .....	6
2. K–Ar standard and airshot data .....	11
3. XRD data .....	17
4. Illite crystallinity (KI) .....	17
5. K–Ar data .....	18
6. K–Ar dates and tectonic events .....	18

# Dating Proterozoic fault movement using K–Ar geochronology of illite separated from lithified fault gouge

by

HN Cutten, H Zwingmann<sup>1</sup>, T Uysal<sup>2</sup>, A Todd<sup>2</sup> and SP Johnson

## Abstract

K–Ar dating of authigenic illite in separated fine-grained clay fractions of fault gouge can date a fault's most recent movement event, and possibly older movements. The method has previously been successfully applied to dating Phanerozoic fault movements, but the present study from the Capricorn Orogen in Western Australia is one of the first to date much older (Proterozoic) events. Previous studies using this technique have used Illite Age Analysis to differentiate between 2M<sub>1</sub> illite polytypes from inherited, and dominant in coarser size fractions, and 1M authigenic illite which predominates in finer size fractions. This analysis permits the influence of the former, on the measured isotopic date, to be removed. However, the determination of illite crystallinity by X-ray diffraction is consistent with elevated faulting temperatures that permitted the growth of authigenic 2M<sub>1</sub> as individual grains, or as rims on existing coarse-grained 2M<sub>1</sub>. The K–Ar date of the finest clay fraction is thus interpreted to be authigenic and representative of the most recent fault movement. Coarser size fractions of the same sample may date older authigenic 2M<sub>1</sub> produced during earlier faulting events. The samples dated in this study were recovered from surface exposures or drillcore from the Mount Vernon and Quartzite Well Faults, which deform sedimentary rocks of the Edmund and Collier Groups (1673–1067 Ma), in the Capricorn Orogen. Our study identifies the Kuparr Tectonic Event (885–782 Ma) as well as younger events at c. 664, 346 and 238 Ma, which have not previously been recognized in the Capricorn Orogen.

**KEYWORDS:** Capricorn Orogen, fault gouge, K–Ar dating, Kuparr Tectonic Event, Proterozoic, Rodinia

## Introduction

The Capricorn Orogen of Western Australia is one of the oldest and most studied Proterozoic collisional belts in the world, benefiting from many decades of detailed geological field mapping augmented by integrated remote sensing imagery, geochronology, geochemistry and geophysical data, including the Capricorn Orogen deep crustal seismic reflection survey (Johnson et al., 2013; Cutten et al., 2016). This study is focused on constraining the complex brittle faulting history of 1673–1067 Ma sedimentary rocks of the Edmund and Collier Groups in the Capricorn Orogen. The study has significance for dating very old (Proterozoic) faulting events to shed light on the complex history of a Proterozoic collisional belt. Isotopic dating of faulting events in the shallow crust, which resides in the brittle regime, is difficult because relatively low temperatures prevent the syntectonic recrystallization or growth of mineral chronometers that are commonly present in deeper fault and shear zone systems.

The timing of faulting events in the Edmund and Collier Groups has largely been inferred from the U–Pb dating of zircon, baddeleyite and phosphate minerals that grew during higher-grade deformation events in underlying basement rocks of the Gascoyne Province (Sheppard et al., 2007; Johnson et al., 2011a). The timing of shallow crustal faulting has also been indirectly constrained by the ages of detrital zircons in sedimentary rocks, including some volcanoclastic rocks (e.g. Wingate et al., 2012a), the ages of magmatic zircon and baddeleyite in mafic intrusive rocks (Wingate, 2002; Wingate et al., 2012b), and from the ages of xenotime and monazite in hydrothermally altered rocks in the basins (Zi et al., 2015).

In this study we determined the age of brittle fault movement directly by dating synkinematic illite from fault gouge using the K–Ar method. The exposed Mount Vernon and Quartzite Well Fault systems targeted in this study have similar orientations to pre-existing faults and shear zone networks in the underlying Gascoyne Province basement, and display the shallow crustal response to basement fault reactivation (Cutten et al., 2016). Additionally, these fault systems have acted as major basin structures accommodating both the formation and inversion of the Edmund and Collier Basins.

<sup>1</sup> Department of Geology and Mineralogy, Kitashirakawa Oiwakecho, Sakyo-ku, Kyoto University, Kyoto, 606–8502, Japan

<sup>2</sup> CSIRO Australian Resources Research Centre (ARRC), Kensington WA 6155, Australia

Fault gouge resulting from displacement on discrete fault planes commonly comprises crushed rock fragments and authigenic clay minerals, such as illite, formed by hydration reactions (Viola et al., 2013). In this study, illite has been recovered from lithified fault gouge in exposed faults and from drillcore intersecting fault strands at depth. Numerous studies have highlighted the use of the K–Ar dating method in constraining the timing of brittle deformation and generation of fault gouge in brittle faults (Kralik et al., 1992; van der Pluijm et al., 2001; Zwingmann et al., 2004; Zwingmann and Mancktelow, 2004; Solum et al., 2005; Uysal et al., 2006; Sasseville et al., 2008; Zwingmann et al., 2010a,b; Duvall et al., 2011; Pleuger et al., 2012; Hetzel et al., 2013; Isik et al., 2014; Torgersen and Viola, 2014; Viola et al., 2016; Babaahmadi et al., 2019), although most of these studies are on much younger (Phanerozoic) fault systems. The isotopic signatures of Proterozoic brittle fault rocks can be robust (Viola et al., 2013), and it is possible to constrain the ages of faulting events using a combination of K–Ar dating, structural geology, careful sample separation, and mineralogical characterization tools such as scanning electron microscopy (SEM) and X-ray diffraction (XRD).

K–Ar dating of fine-grained (<0.1  $\mu\text{m}$ ) illite recovered from fault rocks is more suitable than the  $^{40}\text{Ar}/^{39}\text{Ar}$  method due to the known problems associated with Ar recoil; that is, the loss of  $^{39}\text{Ar}$  during neutron creation from  $^{39}\text{K}$  (in the course of  $^{40}\text{Ar}/^{39}\text{Ar}$  dating), which can be as high as 20% in the finer-grain fractions (Clauer et al., 2012). Previous K–Ar studies (van der Pluijm et al., 2001; Uysal et al., 2006; Duvall

et al., 2011; Ring and Gerdes, 2016) have applied Illite Age Analysis (IAA), dating a progressively finer series of clay-size fractions and regressing the isotopic date against the proportion of illite polytype  $2\text{M}_1$  (inherited protolith detrital component). The y-intercept of the regression was interpreted as the date of most recent fault movement, representing 0%  $2\text{M}_1$  (detrital/protolith illite polytype) and 100%  $1\text{M}/1\text{M}_d$  (authigenic illite polytype). This method was originally developed by Pevear (1999) to determine hydrocarbon source maturity, and has been successfully applied to younger fault systems but only rarely attempted with Proterozoic fault systems (Thébaud and Zwingmann, 2012; Viola et al., 2013). In the present study, K–Ar dates were obtained for a very fine fraction, ideally <0.1  $\mu\text{m}$ , and a coarser fraction (>2  $\mu\text{m}$ ). The finest fraction is interpreted to date the most recent movement on the fault (Torgersen et al., 2015). The coarser size, measured for reference, is interpreted as dating largely protolith illite/muscovite  $2\text{M}_1$  polytype, or may represent an older faulting event (e.g. Viola et al., 2016). This case study demonstrates the potential of the K–Ar technique for dating fault movement in other Proterozoic orogens.

## Geological setting

The Proterozoic Edmund and Collier Basins are the youngest depositional elements of the Capricorn Orogen in Western Australia (Fig. 1). The Capricorn Orogen records the

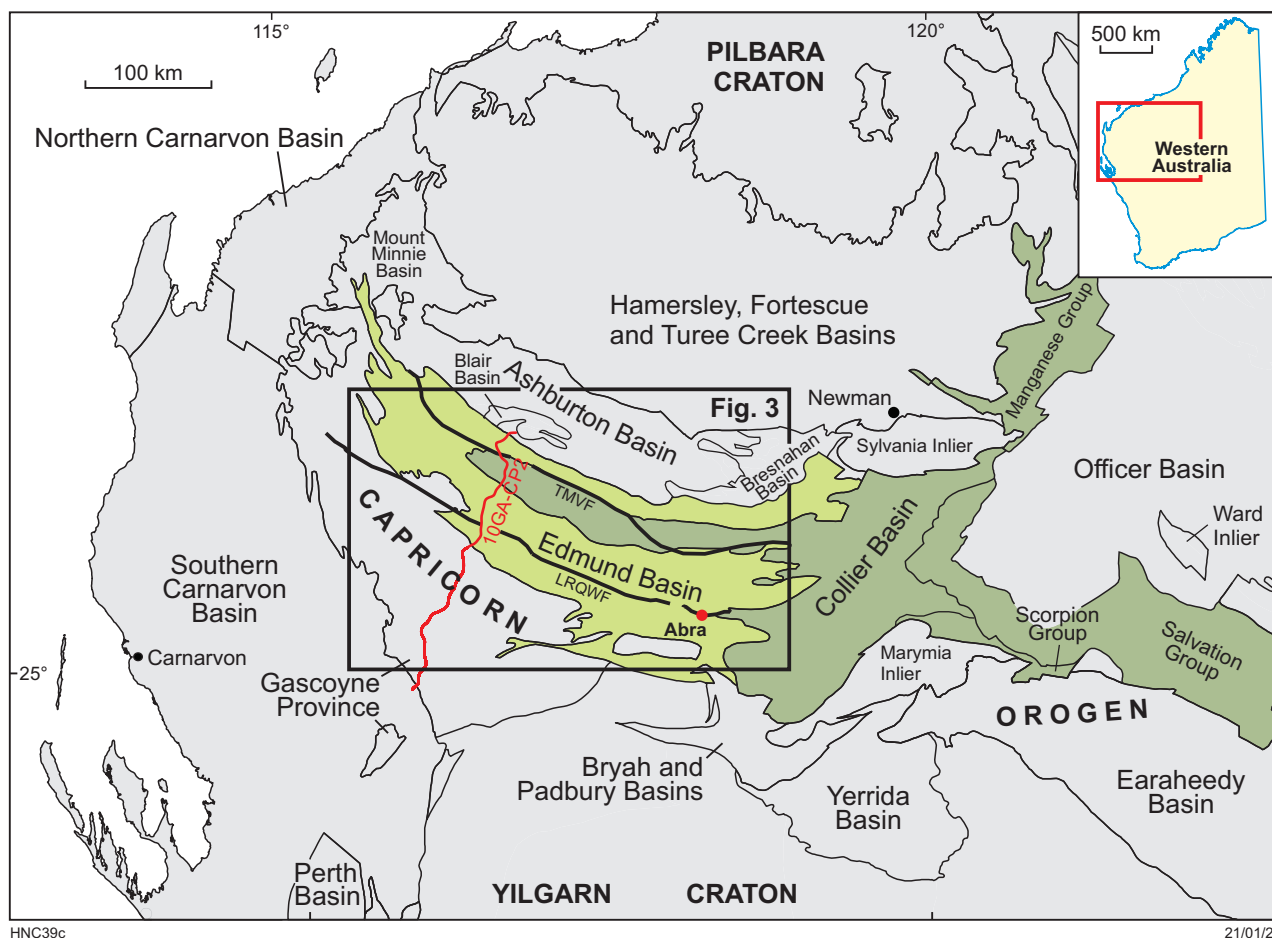


Figure 1. Location of the Edmund and Collier Basins, and older sedimentary basins, in the Capricorn Orogen. Note the location of the Capricorn Orogen deep crustal seismic reflection survey 10GA-CP2, and the Abra polymetallic deposit. Dated faults are the Mount Vernon Fault system which connects to the Talga Fault to the west (TMVF) and the Quartzite Well Fault system which connects to the Lyons River Fault to the west (LRQWF)

Proterozoic assembly of the West Australian Craton from three continental domains (Johnson et al., 2011a). These are, from north to south, the Archean Pilbara Craton, the exotic Archean to Paleoproterozoic Glenburgh Terrane, and the Archean Yilgarn Craton. Paleoproterozoic assembly of the West Australian Craton took place during the 2215–2145 Ma Ophthalmia and 2005–1950 Ma Glenburgh Orogenies, followed by two tectonomagmatic events: the 1820–1770 Ma Capricorn Orogeny (Sheppard et al., 2010) and the 1680–1620 Ma Mangaroon Orogeny (Sheppard et al., 2005, 2010). Crustal-scale faults and shear zones that formed during these events appear to have fundamentally controlled the formation and subsequent inversion of the Mesoproterozoic Edmund and Collier Basins (Cutten et al., 2016). In these basins, the southeast- to east-trending, south-dipping faults and shear zones are steep at the surface, but more gently dipping at depth or are distinctly listric, as imaged in the deep crustal seismic reflection survey (10GA-CP2; Fig. 1). Initially normal faults, they were reactivated as thrusts or transpressional faults (Cutten et al., 2016). They are spatially associated with metalliferous ore bodies, principally stratabound lead, copper, gold and silver, but also including occurrences of rare earth elements, manganese, uranium and diamond (Cutten et al., 2016).

Sedimentary rocks of the Edmund and Collier Groups (Fig. 2) were described by Martin and Thorne (2004) who established the stratigraphic succession as a series of depositional packages defined by basal unconformities or major marine flooding surfaces. The timing of basin formation and deposition is currently constrained by U–Pb dating of detrital zircons (Martin et al., 2008), as well as by U–Pb dating of magmatic zircons from volcanoclastic rocks, and magmatic zircon and baddeleyite from younger mafic sills emplaced within the sedimentary succession (Wingate et al., 2014; Blay et al., 2018). The 1673–1455 Ma Edmund Group and the overlying 1298–1067 Ma Collier Group (Martin and Thorne, 2004; Martin et al., 2008; Cutten et al., 2016) comprise packages of mixed siliciclastic and carbonate sedimentary rocks, which were deposited in a variety of sedimentary environments.

The depositional architecture of the Edmund Basin appears to have been controlled principally by the reactivation of pre-existing, major crustal structures in the underlying Gascoyne Province basement; in particular, the Mount Vernon and Quartzite Well Faults and their continuations to the west, the Talga and Lyons River Faults, respectively (Fig. 1; Martin and Thorne, 2004; Cutten et al., 2016). These structures were interpreted from geological mapping (Martin and Thorne, 2004; Cutten et al., 2016) and imaged by the Capricorn Orogen deep crustal seismic reflection survey (Johnson et al., 2013) as listric, south-dipping faults that form a half-graben architecture. The Talga – Mount Vernon Fault separates the Edmund Basin from the Pingandy Shelf and the Pilbara Craton basement to the north and was the principal basin-forming structure (Cutten et al., 2016). The Lyons River Fault offsets the Moho and is interpreted to be the suture zone between the Pilbara Craton and the Glenburgh Terrane (Johnson et al., 2013). The Lyons River Fault continues to the east as the Quartzite Well Fault, which lies adjacent to the major, stratabound, polymetallic 1610–1590 Ma Abra deposit (Zi et al., 2015). The Lyons River – Quartzite Well Fault system has been interpreted as a mantle tapping structure which acted as a conduit for hydrothermal and mineralizing fluids (Johnson et al., 2013; Zi et al., 2015).

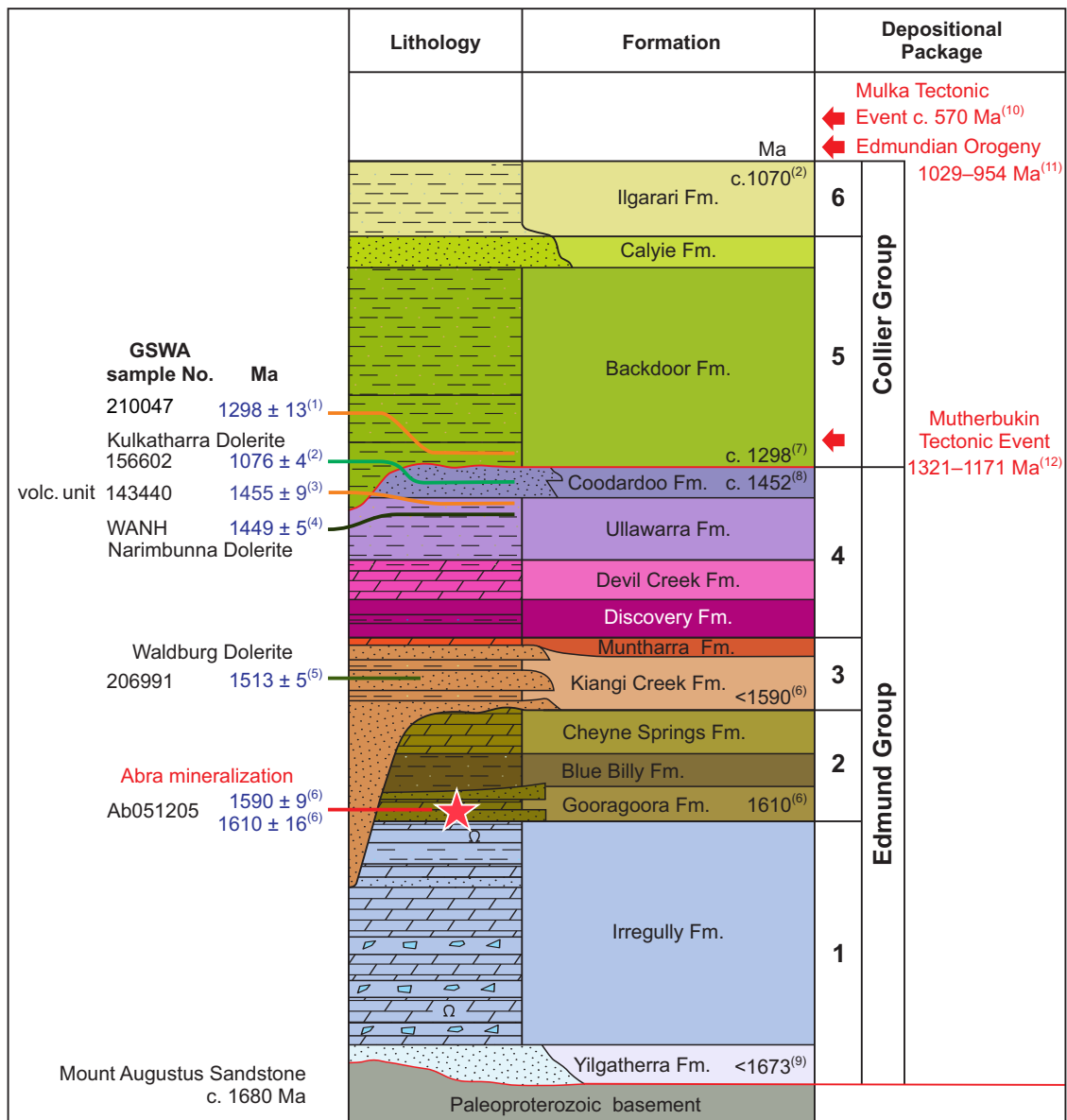
Given the importance of the Talga – Mount Vernon and Lyons River – Quartzite Well Fault systems (Cutten et al., 2016), thirteen samples of fault rocks were recovered for K–Ar dating to directly determine their fault movement history. Nine of these samples were suitable for K–Ar illite dating. The K–Ar dates identify the most recent fault movements, some of which were previously unrecognized.

## Timing of reactivation events in basement rocks of the Gascoyne Province

Dating syntectonic metamorphic and hydrothermal minerals in the medium- to high-grade basement rocks of the underlying Gascoyne Province has defined the major tectonic events of the Capricorn Orogeny (Fig. 3, Table 1). Magmatic and metamorphic ages from SHRIMP U–Pb dating of zircon and phosphate minerals also record the timing of punctuated reactivation of older shear zones and sutures in these basement rocks. Two of the younger N–S compressional reactivation events, the 1321–1171 Ma Mutherbukin Tectonic Event and the 1026–954 Ma Edmundian Orogeny, were largely responsible for the faulting and folding of sedimentary rocks in the Edmund and Collier Basins. Deformation of the basins by two younger events, the 885–782 Ma Kuparr Tectonic Event and the c. 570 Ma Mulka Tectonic Event, is more cryptic.

### Mutherbukin Tectonic Event

The 1321–1171 Ma Mutherbukin Tectonic Event affected basement rocks primarily in the central Gascoyne Province (Johnson et al., 2011b; Korhonen et al., 2015, 2017). The primary expression of the event is a strong upright schistosity or crenulation schistosity in metasedimentary rocks, and a well-developed foliation or gneissic banding in metamorphosed granitic rocks. SHRIMP U–Pb dating of monazite, xenotime and zircon from pelitic schists and granitic gneisses indicates that medium- to high-grade metamorphism, sinistral N–S transpression, and thin-skinned crustal thickening occurred between c. 1321 and 1270 Ma. The thermal effects of this event lasted for more than 100 Ma, with estimates of peak metamorphism defining an apparent thermal gradient of 45 °C/km, and the heat source identified was primarily thickening of radiogenic crust (Korhonen et al., 2015). Peak metamorphism was terminated by transtension and crustal thinning from c. 1210 to 1171 Ma. The maximum age of the event is constrained by a U–Pb date of 1321 ± 40 Ma (GSWA 195826, Wingate et al., 2013) from abundant metamorphic rims on igneous zircon cores in granitic rocks of the Davey Well Granite (Korhonen et al., 2015). The minimum age of the event is constrained by a U–Pb date of 1171 ± 4 Ma (GSWA 88475, Sheppard et al., 2007; Korhonen et al., 2015, 2017) for monazite in hydrothermally altered pelitic schist at the contact with a pegmatite dyke (Fig. 3, Table 1). Other U–Pb dates between the maximum and minimum constraints were obtained from the basement rocks and are summarized in Table 1. Similar dates have also been recorded from the Edmund Basin, and from within the Abra polymetallic deposit.



HNC62

28/01/21

Figure 2. Stratigraphy of the Edmund and Collier Groups showing subdivision into depositional packages and formations, and the timing of tectonic events determined from dating of underlying basement rocks. Dating of the stratigraphy of the Edmund and Collier Groups has been defined by detrital zircons (indicating maximum depositional ages), and by dating of zircons from volcanoclastic sediments and mafic intrusions (Waldburg, Narimbunna and Kulkatharra Dolerites indicating minimum ages), as well as dated Abra mineralization.

Date references: 1) Wingate et al. (2019); 2) Wingate and Bodorkos (2007); 3) Wingate et al. (2012a); 4) Wingate et al. (2014); 5) Wingate et al. (2015); 6) Zi et al. (2015); 7) Wingate et al. (2019); 8) Wingate et al. (2012c); 9) Wingate et al. (2018); Martin et al. (2008); 10) Bodorkos and Wingate (2007); 11) Sheppard et al. (2007); 12) Korhonen et al. (2015)

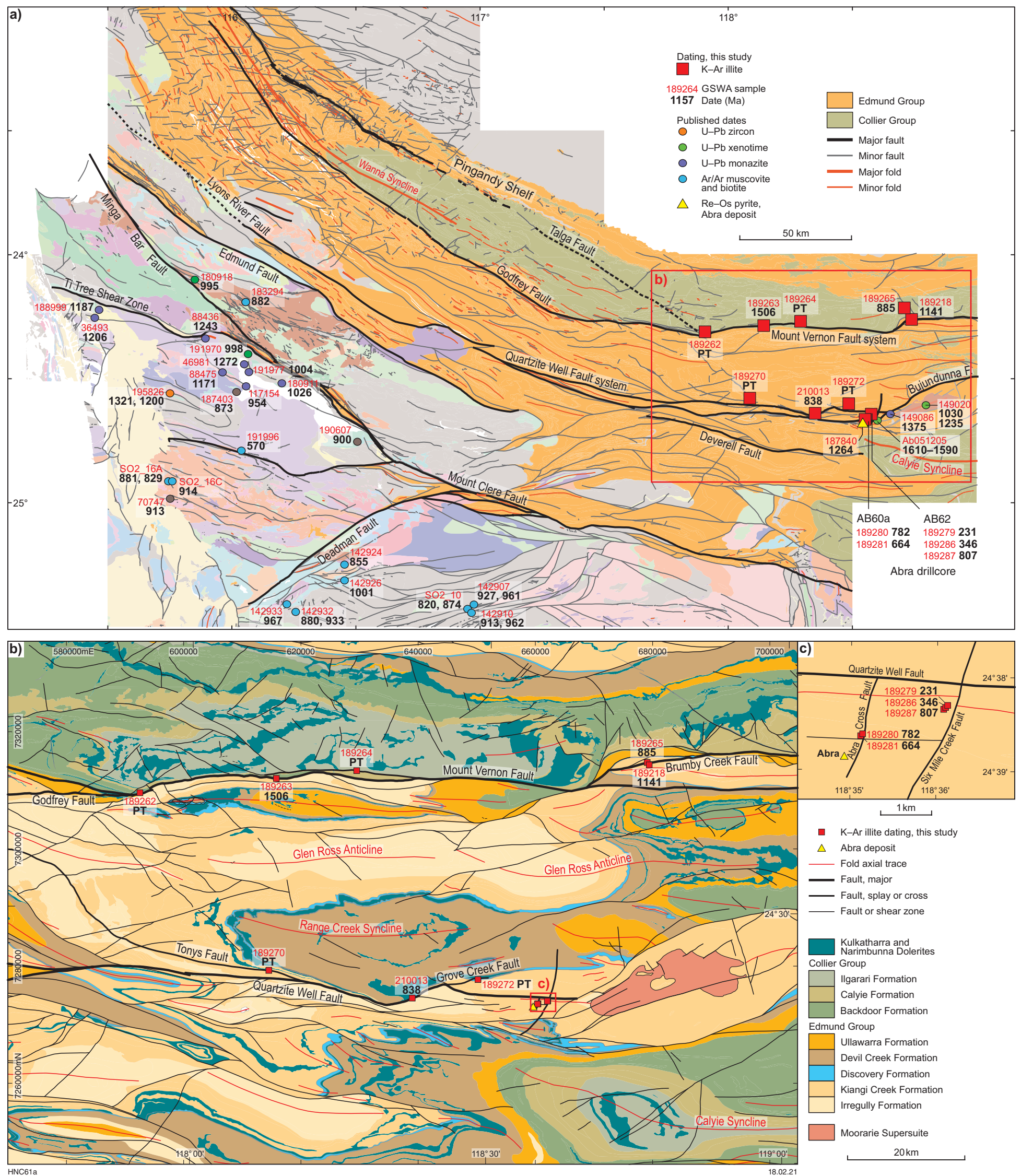


Figure 3. Locations of dated K–Ar samples from the Mount Vernon and Quartzite Well Fault systems: a) K–Ar sample locations, and published U–Pb, Re–Os and Ar/Ar dates from the Edmund and Collier Basins and underlying basement rocks; b) detail of K–Ar sample locations and the sampled faults; c) samples with K–Ar dates close to Six Mile Creek and Abra Cross Faults, and Abra mineral deposit. GSWA sample numbers in red, K–Ar dates in black numerals. PT indicates petrographically examined samples which were not dated

Table 1. Published dates and events

Sample ID	Method	Mineral	Lithology	Date (Ma)	Formation/Unit	Event/Orogeny	Reference
<b>Edmund and Collier Basins</b>							
191996	Ar–Ar	white mica	mylonite	570 ± 10	Chalba Shear Zone	Mulka	Bodorkos and Wingate (2007)
189289	U–Pb	monazite	unmineralized sandstone	995 ± 18	Abra core (AB62)	Edmundian	Zi et al. (2015)
149020	U–Pb	xenotime rim	rhyolite	1030 ± 40	Tangadee Rhyolite	Edmundian	Rasmussen et al. (2010)
189293	U–Pb	monazite	hydrothermal red zone	1221 ± 14	Abra core (AB62)	Mutherbukin	Zi et al. (2015)
149020	U–Pb	xenotime	rhyolite	1235 ± 19	Tangadee Rhyolite	Mutherbukin	Rasmussen et al. (2010)
187840	Re–Os	pyrite	hydrothermal red zone	1284 ± 47	Abra core	Mutherbukin	Pirajno et al. (2010)
156589	U–Pb	monazite	sandstone	1300 ± 10	Mount Augustus Sandstone	Mutherbukin	Rasmussen (preliminary data)
149086	U–Pb	monazite	hydrothermal red zone	1375 ± 14	Abra core (AB58)	local event	Zi et al. (2015)
AB051205	U–Pb	xenotime	hydrothermal black zone	1594 ± 10	Abra core (AB16)	mineralizing event	Zi et al. (2015)
AB051205	U–Pb	xenotime	hydrothermal black zone	1610 ± 16	Abra core (AB16)	mineralizing event	Zi et al. (2015)
<b>Gascoyne Province</b>							
S02_10 gr1	Ar–Ar	biotite	granitic gneiss	820 ± 14	Warrigal Gneiss	960–820 Ma (min) exhumation event	Occhipinti et al. (2007)
S02_10 gr2	Ar–Ar	biotite	granitic gneiss	874 ± 11	Warrigal Gneiss	960–820 Ma exh.	Occhipinti et al. (2007)
S02_16A gr1	Ar–Ar	muscovite	low-grade metaconglomerate	881 ± 15	Mount James Formation	960–820 Ma exh.	Occhipinti et al. (2007)
S02_16A gr2	Ar–Ar	muscovite	low-grade metaconglomerate	829 ± 15	Mount James Formation	960–820 Ma exh.	Occhipinti et al. (2007)
S02_16C	Ar–Ar	muscovite	low-grade metaconglomerate	914 ± 4	Mount James Formation	960–820 Ma exh.	Occhipinti et al. (2007)
142907	Ar–Ar	biotite	monzogranite dyke	927 ± 23	Errabiddy Shear Zone	960–820 Ma exh.	Occhipinti et al. (2007)
142907	Ar–Ar	muscovite	monzogranite dyke	961 ± 4	Errabiddy Shear Zone	960–820 Ma exh.	Occhipinti et al. (2007)
142910	Ar–Ar	biotite	migmatized pelite	962 ± 10	Camel Hills Metamorphics	960–820 Ma exh.	Occhipinti et al. (2007)
142910	Ar–Ar	muscovite	migmatized pelite	913 ± 20	Camel Hills Metamorphics	960–820 Ma exh.	Occhipinti et al. (2007)
142932	Ar–Ar	muscovite	granite	880 ± 4	Dalgaringa Supersuite	960–820 Ma exh.	Sheppard et al. (2004) Occhipinti et al. (2007)
142932	Ar–Ar	biotite	granite	933 ± 33	Dalgaringa Supersuite	960–820 Ma exh.	Occhipinti et al. (2007)
142924	Ar–Ar	biotite	granite	855 ± 3	Moorarie Supersuite	960–820 Ma exh.	Occhipinti et al. (2007)
142926	Ar–Ar	biotite	granite	1001 ± 16	Dalgaringa Supersuite	960–820 Ma exh.	Occhipinti et al. (2007)
142933	Ar–Ar	biotite	granulite facies metadiorite	967 ± 6	Dalgaringa Supersuite	960–820 Ma (max) exhumation event N–S compression	Sheppard et al. (2004) Occhipinti et al. (2007)
183294	Ar–Ar	muscovite	quartz mylonite	882 ± 3	Minnie Creek Batholith	N–S compression	Piechocka et al. (2018)
216533	Ar–Ar	biotite	biotite–garnet schist	908 ± 3	Durlacher Supersuite	low-grade metam.	Piechocka et al. (2018)
190607	U–Pb	rutile	pelitic schist	900 ± 8	Leake Springs Metamorphics	low-grade metam..	Olierook et al. (2019)
70747	U–Pb	rutile	metasiltstone	913 ± 8	Dalgaringa Supersuite	low-grade metam.	Olierook et al. (2019)
187403	U–Pb	rutile	quartzite	873 ± 8	Moogie Metamorphics		Olierook et al. (2019)
UWA117154	U–Pb	monazite	rare element pegmatite	954 ± 12	Nardoo Granite	Edmundian (min)	Sheppard et al. (2007)
180918	U–Pb	xenotime	schist	995 ± 6	Pooranoo Metamorphics	Edmundian	Sheppard et al. (2007)
1191970	U–Pb	xenotime	schist	998 ± 8	Pooranoo Metamorphics	Edmundian	Sheppard et al. (2007)
191977	U–Pb	monazite	schist	1004 ± 12	Leake Springs Metamorphics	Edmundian	Sheppard et al. (2007)
180911	U–Pb	monazite	schist	1005 ± 10	Leake Springs Metamorphics	Edmundian	Sheppard et al. (2007)
180911	U–Pb	monazite	schist	1026 ± 12	Leake Springs Metamorphics	Edmundian (max)	Sheppard et al. (2007)
88475	U–Pb	monazite	pelitic schist	1171 ± 4	Tommie Well (location)	Mutherbukin (min)	Sheppard et al. (2007) Korhonen et al. (2015)
188999	U–Pb	monazite	metasedimentary and meta-igneous	1187 ± 7	Nik Belt, Mutherbukin Zone	Mutherbukin	Korhonen et al. (2015)
195826	U–Pb	zircon rim	monzogranite	1200 ± 3	Davey Well Granite	Mutherbukin	Wingate et al. (2013)
36493	U–Pb	monazite	metasedimentary and meta-igneous	1206 ± 6	Nik Belt, Mutherbukin Zone	Mutherbukin	Korhonen et al. (2015)
88436	U–Pb	monazite	pelitic schist	1243 ± 7	Tommie Well (location)	Mutherbukin	Korhonen et al. (2015)
46981	U–Pb	monazite	pelitic schist	1272 ± 9	Nardoo Well (location)	Mutherbukin	Korhonen et al. (2015)
88436	U–Pb	monazite	pelitic schist	1281 ± 3	Tommie Well (location)	Mutherbukin	Korhonen et al. (2015)
195826	U–Pb	zircon rim	monzogranite	1321 ± 40	Davey Well Granite	Mutherbukin (max)	Wingate et al. (2013)

These include a U–Pb date of  $1235 \pm 19$  Ma from a probable hydrothermal xenotime core of the Tangadee Rhyolite of the Kiangi Creek Formation (GSWA 149020, Rasmussen et al., 2010), and a Re–Os date of  $1284 \pm 47$  Ma (GSWA 187840, Pirajno et al., 2010) from pyrite within the mineralized red zone of the Abra deposit. An older date of  $1385 \pm 20$  Ma obtained from authigenic monazite within the Abra ore zone (GSWA 149086, Rasmussen et al., 2010) was recalculated by Zi et al. (2015) at  $1375 \pm 14$  Ma, and has been interpreted to represent an early phase of hydrothermal activity preceding the Mutherbukin Tectonic Event.

## Edmundian Orogeny

The 1026–954 Ma Edmundian Orogeny post-dates the Collier Group and has deformed both the Edmund and the Collier Basins. The Edmundian Orogeny was responsible for regional greenschist to amphibolite facies metamorphism and deformation, granitic magmatism, and pegmatite intrusion in the basement rocks of the Gascoyne Province (Sheppard et al., 2007). The structural trends of the Edmundian Orogeny and Mutherbukin Tectonic Event are essentially subparallel, making it difficult to differentiate between the two (Cutten et al., 2016). The maximum age for the Edmundian Orogeny is derived from a SHRIMP U–Pb monazite date of  $1026 \pm 12$  Ma (GSWA 180911, Sheppard et al., 2007) from amphibolite facies rocks (Fig. 3, Table 1). The minimum age is derived from a U–Pb monazite date of  $954 \pm 12$  Ma (UWA\* sample 117154, Sheppard et al., 2007) for an undeformed pegmatite dyke that crosscuts Edmundian-age fabrics. Other dates that fall between the maximum and minimum constraints for this event are summarized in Table 1.

## Kuparr Tectonic Event

The 885–782 Ma age of the Kuparr Tectonic Event, named by Cutten and Johnson (2018), is constrained by the K–Ar geochronology presented in this Report. Metamorphic muscovite and biotite from greenschist facies rocks in the southern Gascoyne Province yielded mostly poorly defined  $^{40}\text{Ar}/^{39}\text{Ar}$  dates between c. 960 and 820 Ma (Occhipinti, 2007). These dates were identified as representing cooling through a closure temperature of 270–350 °C (Occhipinti, 2007) and were suggested to represent a regional-scale exhumation event. Similar dates of 920–830 Ma were reported from  $^{40}\text{Ar}/^{39}\text{Ar}$  dating of mica and U–Pb dating of xenotime from shear zones in basement rocks across the Gascoyne Province (Piechocka et al., 2018). These dates were interpreted to reflect north–south compression and dextral strike-slip reactivation of pre-existing faults and shear zones. U–Pb dates between c. 913 and 873 Ma for hydrothermally altered rutile, together with the existing mica and xenotime dates, were used to describe a period of very low- to low-grade metamorphism, metasomatism, minor leucocratic and pegmatitic magmatism, and reactivation of northwest-trending faults between c. 955 and 830 Ma (Olierook et al., 2019).

## Mulka Tectonic Event

A series of anastomosing shears, part of the Chalba Shear Zone in basement rocks of the Gascoyne Province, displays consistent dextral strike-slip movement and offsets dykes of the c. 755 Ma Mundine Well Dolerite (Wingate and Giddings, 2000). White mica in the S-planes of S–C fabrics in shear zone mylonite yielded an  $^{40}\text{Ar}/^{39}\text{Ar}$  date of  $570 \pm 10$  Ma (Bodorkos and Wingate, 2007) interpreted as the age of the Mulka Tectonic Event (Fig. 3, Table 1).

## Sample collection

Displacement of geological units identified by geological mapping and additional interpretation of magnetic anomaly imagery indicates that the Edmund and Collier Basins are cut by numerous brittle faults. Their surface expressions are typically limited to offset ridges of silicified sandstone with intervening valleys filled with colluvial regolith (Fig. 4a), or the faults appear as linear outcrops of quartz veins (Fig. 4b). Lithified fault gouge was recovered from rare surface exposures of fault rocks (Fig. 4c). Shear planes showing slickenlines are more numerous (Fig. 4d), and some of these are located within quartz-ironstone breccia marking the fault trace (Fig. 4e). Some of the slickenlines were sampled, although the absence of slickenfibres meant these samples to be unsuitable for K–Ar dating. The sense of fault movement, most commonly reverse or transpressive, could be recorded from slickenlines only on rocks clearly identified as in situ. Additional samples were obtained from drillcore from two drillholes (Abra Mining Ltd, core recovered in 2012) that intersected strands of the Quartzite Well Fault. These are the Six Mile Creek Fault (drillcore AB62; Fig. 5a) and the Abra Cross Fault (AB60a; Fig. 5b). In addition, a whole-rock sample of undeformed host rock was also dated to investigate any possible authigenic minerals that might be present in the deformed examples.

## Mount Vernon Fault system

The Mount Vernon Fault system and the connecting Talga Fault to the west (Fig. 3) extends for more than 400 km. Samples were recovered from five localities. Two fault strands (the North and South Brumby Creek Faults), which are parallel to the Mount Vernon North Splay Fault, are well exposed in a small creek on a vertical, east-facing cliff. The South Brumby Creek Fault shows reverse offset of about 20 cm of the well-bedded, 1–10 cm-thick alternating beds of siltstone and sandstone of the Kiangi Creek Formation (Edmund Group). The fault plane dips 35° towards an azimuth of 230° and includes a well-developed, 5 cm-thick fault gouge (sample GSWA 189218; Figs 3b, 4c). The North Brumby Creek Fault, 5 m to the north, shows 25 cm of reverse offset, dips 45° towards 355° and includes a 1 cm-wide fault gouge (sample GSWA 189265; Fig. 3b).

\* Numbers prefixed by UWA refer to The University of Western Australia sample collection

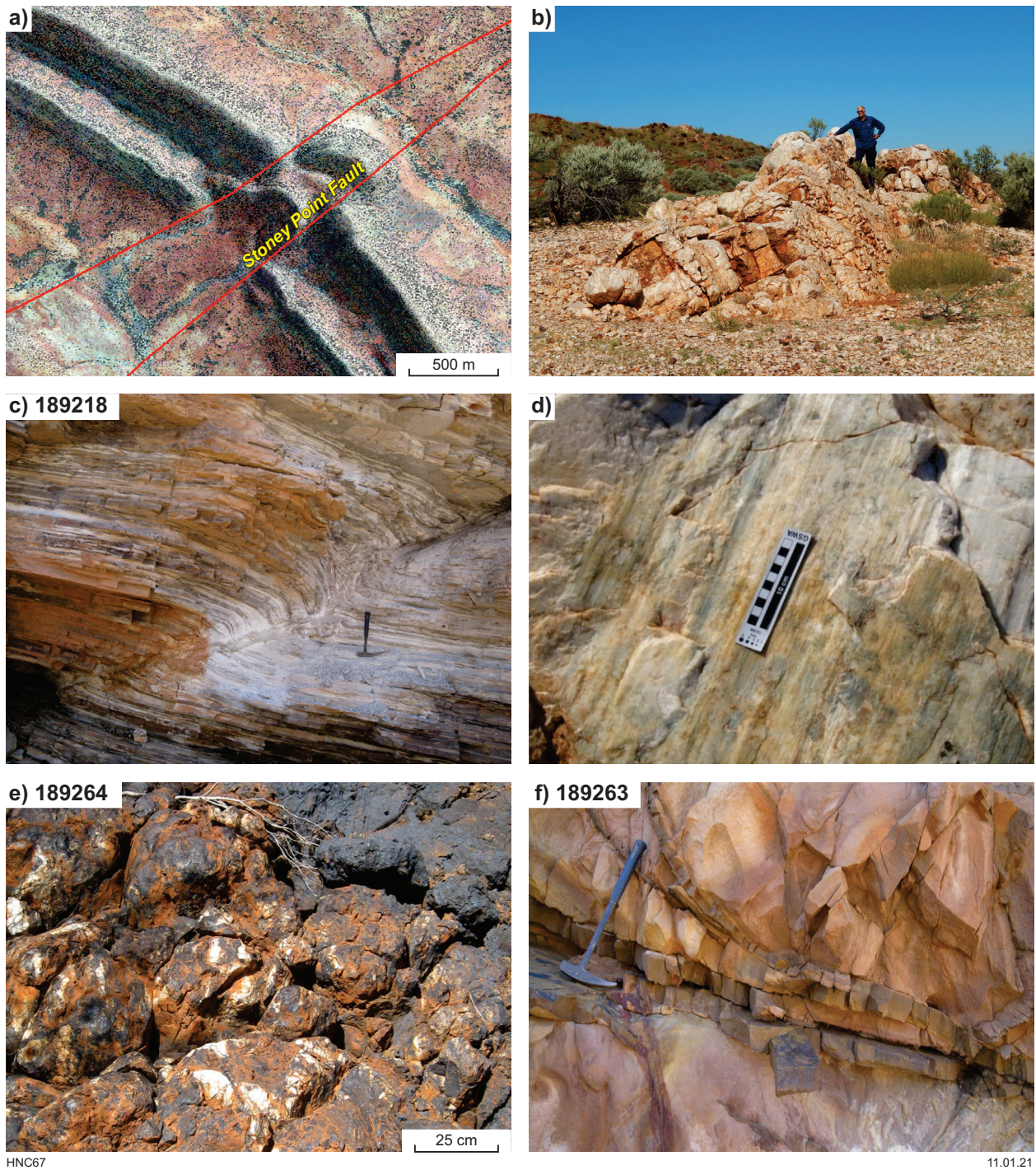


Figure 4. Surface expressions of faulting in the Edmund and Collier Groups: a) shaded orthophoto image showing fault displacement of sandstone ridges of the Calyie Formation (Collier Group). This represents the Edmundian Orogeny or more recent fault movement; b) linear quartz vein, undated; c) exposed fault showing reverse displacement, located on the South Brumby Creek Fault (Mount Vernon Fault system). Fault gouge sample (0.2 – 0.1  $\mu\text{m}$  fraction; GSWA 189218) dated at  $1141.2 \pm 58.6$  Ma; Mutherbukin Tectonic Event fault movement; d) example of slickenlines indicating reverse displacement; e) fault breccia, Mount Vernon Fault system (sample GSWA 189264); f) sheared siltstone of the Kiangi Creek Formation (sample GSWA 189263), whole-rock dated at  $1506.6 \pm 30.2$  Ma (depositional age, modified by authigenic mineral growth associated with shearing)

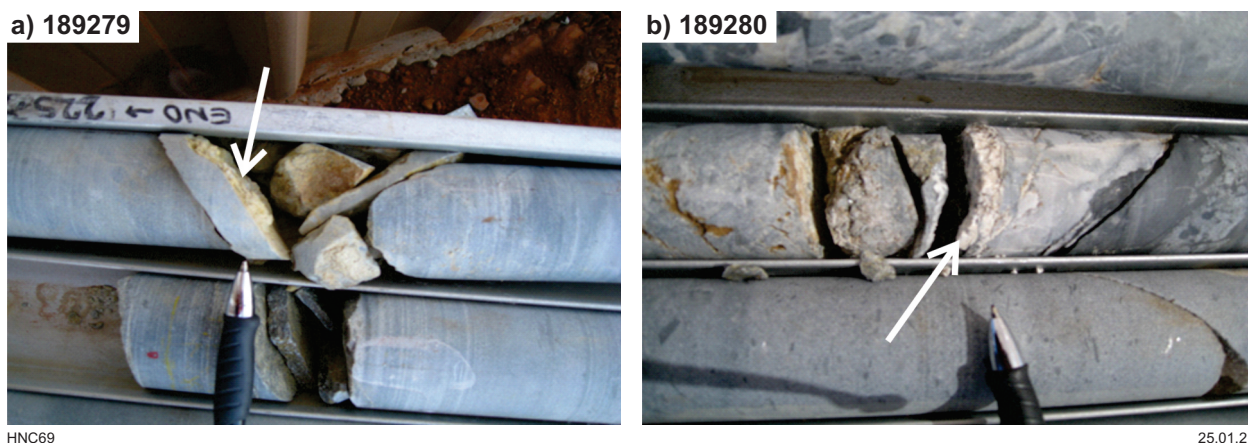


Figure 5. Abra drillcore showing lithified fault gouge sampled for K–Ar dating: a) drillcore AB62, 150 m depth, Six Mile Creek Fault, sample GSWA 189279 (<math><0.1 \mu\text{m}</math> fraction) dated at  $238.1 \pm 5.6$  Ma; b) drillcore AB60a, 216.8 m depth, Abra Cross Fault, sample GSWA 189280 (1 to <math><0.1 \mu\text{m}</math> fraction) dated at  $782.2 \pm 40.1$  Ma

About 50 km to the west, a small branch fault of the Mount Vernon Fault exhibits 20 cm normal offset of weathered siltstone of the Calyie Formation (Collier Group). Suitable material for dating could not be sampled directly from this exposed fault, but a sample (GSWA 189264; Fig. 3b) was obtained from an adjacent rotated block of quartz breccia and ironstone with well-developed slickenlines. A sample of host rock (GSWA 189263; Fig. 4f) was recovered a farther 14 km to the west (Fig. 3b). The exposed rock is sheared sandstone of the Kiangi Creek Formation (Edmund Group). Near the junction of the Mount Vernon and Godfrey Faults (Fig. 3), sample GSWA 189262 was recovered from a slickenside surface on a tightly folded silicified breccia within strongly cleaved ferruginous siltstone of the Backdoor Formation (Collier Group). The slickenside surface dips  $60^\circ$  towards  $165^\circ$  with slickenlines plunging  $60^\circ$  towards  $165^\circ$  showing reverse sense of movement.

## Quartzite Well Fault system

The Quartzite Well Fault system is located in the central Edmund Basin about 30 km south of the Mount Vernon Fault (Fig. 3). The Quartzite Well Fault system comprises a series of strand and branch faults that connect to the west with the northwest-trending Lyons River Fault. Samples were recovered from rare exposures of the Quartzite Well Fault as well as from branch faults, including from two drillcores intersecting the Six Mile Creek and Abra Cross Faults.

Tonys Fault is parallel to, and about 1 km north of, the main Quartzite Well Fault. A sample of in situ fault slickenside (GSWA 189270) was recovered from brecciated, cherty, yellow-brown siltstone of Kiangi Creek Formation (Edmund Group). Slickenlines plunging  $42^\circ$  towards  $349^\circ$  show reverse sense of movement on the fault surface (dipping  $45^\circ$  towards  $345^\circ$ ). A fault gouge sample (GSWA 210013) was recovered from a bedding-parallel fault strand of the Quartzite Well Fault. This fault strand marks the weathered contact of steeply dipping, parallel-planar laminated,

silicified siltstone of the Irregularly Formation (Edmund Group) with boudinaged, wavy laminated, bedded, black chert of the Discovery Formation (Edmund Group). The sense of movement could not be determined. The Quartzite Well Fault system trends northeast from this point and 6 km to the east splits into two strands (Fig. 3). The Grove Creek Fault shows a 150 m apparent dextral offset of the contact between Kiangi Creek and Discovery Formations (Edmund Group). A sample of fault gouge (GSWA 189272) was recovered from parallel-planar laminated, cherty siltstone of the Discovery Formation in a fault zone showing a one-metre reverse displacement and tight drag folds adjacent to the fault. The fault dips  $25^\circ$  towards  $200^\circ$ .

Close to the Abra polymetallic mineral deposit, exploratory diamond drillholes AB62 and AB60a were drilled by Abra Mining Company Ltd to gain a greater understanding of the hydrothermal mineralizing processes which produced the deposit. Drillhole AB62, which is located about 450 m south of the Quartzite Well Fault, intersected fine- to medium-grained sandstone of the Kiangi Creek Formation (Edmund Group) and contains splays of the Six Mile Creek Fault. Samples of fault gouge were recovered from depths of 150.00 m (GSWA 189279; Fig. 5a), 396.70 m (GSWA 189286), and 443.72 m (GSWA 189287). The sense of movement could not be determined for the Six Mile Creek Fault.

Drillhole AB60a is located 1.8 km southwest of AB62 and about 1.1 km south of the Quartzite Well Fault. The drillcore intersected the Abra Cross Fault in silicified, fine-grained sandstone of the Kiangi Creek Formation (Edmund Group) that makes a sharp contact with underlying very coarse-grained sandstone and conglomerate fluvial facies of the Gooragoora Formation (Edmund Group). The Gooragoora Formation hosts the mineralized red zone (Pirajno et al., 2010) containing hematite and chalcopyrite of the Abra deposit. Two samples of fault gouge were collected from thin splays of the Abra Cross Fault at depths of 216.8 m (GSWA 189280; Fig. 5) and 225.0 m (GSWA 189281).

## Analytical methods

### Sample processing

Of the 13 selected fault rock samples, nine were suitable for K–Ar dating. The nine samples were loaded into a cryostat chamber for sample disintegration using a gentle heating–freezing method (Liewig et al., 1987). The  $>2\ \mu\text{m}$  and  $<2\ \mu\text{m}$  size fractions were obtained by gravity settling. However, due to the degree of silicification, cryostat disintegration failed for three samples which were subsequently crushed as whole-rock splits using a ring mill. From this, a sample split of  $\sim 1\ \text{g}$  was washed with deionized water and dried overnight at  $60\ ^\circ\text{C}$ . The clean rock was crushed with a ring mill (Siebtechnik ring grinder with chrome steel barrel) to  $750\ \mu\text{m}$ . The  $<2\ \mu\text{m}$  fractions obtained were processed further by centrifuge separations to obtain size fractions as fine as  $<0.1\ \mu\text{m}$ . In each case the separated residue was washed with deionized water into a small ceramic crucible, dried overnight at  $60\ ^\circ\text{C}$ , and the dry power used for X-ray diffraction (XRD) mineralogy examination and K–Ar dating.

### Petrography

Thin sections of fault rocks were examined initially with a petrographic microscope (binocular Leitz Leica DM750P equipped with a mounted camera, Microsystem CH943). While some of the components were too small to be identified by optical mineralogy, the overall composition, alteration and structure of the rock were determined. Representative samples are described in the results section.

### Scanning electron microscopy

Freshly broken surfaces of rock chips were gold coated and examined in secondary electron mode using a Zeiss EVO 40XVP SEM equipped with an energy dispersive X-ray analyser system, (EDS).

### Transmission electron microscopy

A JEOL 2010 TEM was used for detailed, grain-by-grain morphological characterization of selected clay fractions. Samples were prepared by placing one drop of clay solution on a micro-carbon grid film and drying in air. The chemical compositions of individual particles were investigated by an attached EDS system.

### X-ray diffraction

For whole-rock XRD analysis, the powdered samples were sprinkled onto silica low-background sample holder disks and gently pressed flat. XRD patterns were recorded with a PANalytical X'Pert Pro Multi-purpose Diffractometer using Fe-filtered  $\text{CoK}\alpha$  radiation, variable divergence slit,  $1^\circ$  antiscatter slit and fast X'Celerator Si strip detector. The diffraction patterns were recorded in steps of  $0.017^\circ$  ( $2\theta$ ) with a 0.5 s counting time per step, and logged to data files for analysis.

For clay mineral XRD analysis, the samples were lightly front-pressed onto silica low-background sample holders. XRD patterns were recorded with a PANalytical X'Pert Pro Multi-purpose Diffractometer using Fe-filtered  $\text{CoK}\alpha$  radiation, variable divergence slit,  $1^\circ$  anti-scatter slit and fast X'Celerator Si strip detector. The diffraction patterns were recorded in steps of  $0.017^\circ$  ( $2\theta$ ) with a 0.5 s counting time per step, and logged to data files for analysis. Quantitative analysis was performed on the XRD data from all bulk samples using the commercial package SIROQUANT from Sietronics Pty Ltd.

### K–Ar dating

The samples were analysed at the K–Ar Geochronology Facility at CSIRO Energy Flagship in Perth, Western Australia. Potassium content was determined in duplicate by atomic absorption (Varian Spectra AA 50) using Cs for ionization suppression. Two sample aliquots, approximately 50 mg each, were dissolved with HF and  $\text{HNO}_3$  (Heinrichs and Hermann, 1990) for each sample. The pooled uncertainty of duplicate K determination of all samples and standards is better than 2% ( $1\sigma$ ). K–Ar measurements were performed using a procedure similar to that described by Bonhomme et al. (1975). Samples were pre-heated at  $80\ ^\circ\text{C}$  under vacuum for several hours to reduce the amount of atmospheric Ar adsorbed onto the mineral surfaces during sample handling. The isotope composition of Ar was measured with a VG3600 mass spectrometer. The  $^{38}\text{Ar}$  spike was calibrated against standard biotite GA1550 (McDougall and Harrison, 1999). About 5 mg of sample material was required for Ar analysis. During the course of the study, five HD-B1 (Hess and Lippolt, 1994) and two LP-6 (Odin, 1982) international Ar standards, and five airshots, were analysed. The uncertainty of the Ar analysis is better than 1% and the mean  $^{40}\text{Ar}/^{36}\text{Ar}$  value of five airshots (small amounts of air for  $^{40}\text{Ar}/^{36}\text{Ar}$  ratio measurement) is  $295.12 \pm 0.37$  ( $2\sigma$ ; Table 2). K–Ar dates were calculated using  $^{40}\text{K}$  abundance and decay constants recommended by Steiger and Jäger (1977). Age uncertainties are quoted with  $2\sigma$  uncertainties that include contributions from sample weighing,  $^{38}\text{Ar}/^{36}\text{Ar}$  and  $^{40}\text{Ar}/^{38}\text{Ar}$  measurements, and K analysis.

### Illite polytypes

Fault rocks commonly contain two polytypes of illite,  $1\text{M}/1\text{M}_d$  and  $2\text{M}_1$ , which represent different types of crystallographic stacking and are apparent in XRD charts (Fig. 6). The  $1\text{M}/1\text{M}_d$  polytype is diagnostic of authigenic illite (the 1M has a higher crystallinity than  $1\text{M}_d$ , which may also contain smectite). Both are commonly referred together as  $1\text{M}/\text{M}_d$  illite, or just 1M). The  $2\text{M}_1$  polytype is typically diagnostic of detrital (inherited) mica (high-temperature  $>250\ ^\circ\text{C}$  illite) (Srodon and Eberl, 1984). Studies of shallow crustal faults that formed at diagenetic temperatures below  $200\ ^\circ\text{C}$  indicate that the illite/muscovite ( $2\text{M}_1$ ) present in the fault rocks is inherited, either detrital or derived from wallrocks, whereas the illite ( $1\text{M}/\text{M}_d$ ) is authigenic and precipitated within the brittle fault zone during faulting (van der Pluijm et al., 2001; Duvall et al., 2011). Some studies, such as the Illite Age Analysis method (IAA), have employed a two-end-member mixing model to quantify the decreasing

**Table 2. K–Ar standard and airshot data**

Standard ID	K	Radiometric <sup>40</sup> Ar	Radiometric <sup>40</sup> Ar	Age	Error	Remark
	(%)	(mol/g)	(%)	(Ma)	(Ma)	(error to reference)
HD-B1-100	7.96	3.3856E-10	93.42	24.37	0.42	+0.66%
HD-B1-108	7.96	3.3877E-10	92.11	24.38	0.37	+0.70%
HD-B1-109	7.96	3.3581E-10	92.98	24.17	0.37	-0.17%
HD-B1-115	7.96	3.3435E-10	90.38	24.07	0.36	-0.58%
HD-B1-120	7.96	3.3717E-10	92.05	24.27	0.37	+0.25%
LP6-123	8.37	1.9270E-09	97.36	128.08	1.89	+0.14%
LP6-129	8.37	1.9262E-09	97.23	128.03	1.87	+0.10%
Airshot ID	<sup>40</sup> Ar/ <sup>36</sup> Ar					
AS96-AirS-1	293.95	+/-				0.53
AS104-AirS-1	295.50					0.30
AS105-AirS-2	296.70					0.35
AS111-AirS-1	293.78					0.29
AS116-AirS-1	295.69					0.36

proportion of 2M<sub>1</sub> in successively finer clay size fractions, to extrapolate graphically to the age of pure authigenic clay (assumed to be 100% 1M/M<sub>d</sub>). However, the formation of authigenic 2M<sub>1</sub> illite at temperatures above 200 °C in diagenetic-to-hydrothermal conditions is also possible (Lonker and Gerald, 1990; Zwingmann et al., 2010a; Clauer et al., 2012; Viola et al., 2013; Mancktelow et al., 2015; Uysal et al., 2020).

Dating of fault rocks in this study was initially limited to only the <2 µm fraction. Additional dating of finer size fractions was undertaken in recognition that the <2 µm fraction could include detrital mica (2M<sub>1</sub> illite polytype) inherited cataclastically from the host rock, and hence yield a mixed and anomalously older date. A method to determine the true date of the most recent fault movement is the Illite Age Analysis (IAA) method. This method has been successfully applied to determine faulting events in Phanerozoic rocks (van der Pluijm et al., 2001). Employing the IAA method, K–Ar dates determined from 2 to <0.1 µm size fractions show progressively younger dates for the finer fractions, showing an inclined age spectrum (e.g. Fig. 6a). The IAA method attributes this to a decrease in the relative proportion of the 2M<sub>1</sub> illite polytype, which is assumed to be cataclastically included mica from the host rock and hence is older than authigenic 1M illite polytype in the dated sample. Regressing these successively younger dates against the proportion of 2M<sub>1</sub> (Fig. 6a) yields a y-intercept (0% 2M<sub>1</sub>) that can be interpreted as the date of the most recent fault movement (Reynolds, 1963). Determining the proportion of 2M<sub>1</sub> for each size fraction on the regression line is critical to determining this y-axis intercept, but is not straight forward and a number of different methods were trialled in this study.

One method, as applied by Grathooff and Moore (1996), uses formulas referencing Velde and Hower (1963), Reynolds (1963), and Maxwell and Hower (1967). These compare, on a randomly oriented sample, the XRD counts (A, peak area) of 2M<sub>1</sub> peaks (at 2.79 and 3.00 Å) and 1M peaks (at 3.07 and 3.66 Å) with that of the combined 2M<sub>1</sub> and 1M peak (at 2.58 Å).

The formulae are:

$$2M_1(\%) = 1.88 + 702 \times [(A_{2.79} \text{ \AA}) / (A_{2.58} \text{ \AA})]$$

$$2M_1(\%) = 3.25 + 335 \times [(A_{3.00} \text{ \AA}) / (A_{2.58} \text{ \AA})]$$

$$1M(\%) = 3.40 + 132 \times [(A_{3.07} \text{ \AA}) / (A_{2.58} \text{ \AA})]$$

$$1M(\%) = 4.98 + 136 \times [(A_{3.66} \text{ \AA}) / (A_{2.58} \text{ \AA})]$$

There should be agreement between the pairs determined for 2M<sub>1</sub> and 1M, and also that 2M<sub>1</sub> and 1M should sum to 100%, assuming the presence of inherited host-rock mica is correct. In applying the method during this study, agreement was not obtained and the method was not applied.

A second technique for determining polytype percentages uses the software WILDFIRE (Grathooff and Moore, 1996). This method applies a visual (on-screen) comparison of generated standard XRD charts of defined 2M<sub>1</sub> and 1M proportions against the user's clay fraction experimentally obtained XRD chart. WILDFIRE allows extensive capability to adjust the parameters of the generated standard XRD charts to most closely match those of the XRD facility operated by the user; for example, XRD tube used (Cu or Co), 2θ angle scan range, as well as more advanced crystallographic parameters. Once these parameters are specified, the user's clay sample XRD chart is compared with standard charts with set 2M<sub>1</sub> and 1M proportions; e.g. 80% 2M<sub>1</sub> and 20% 1M. Intermediate 'standard charts' can be generated by mixing two standard charts. For example, mixing the chart for 80% 2M<sub>1</sub> and 20% 1M with 70% 2M<sub>1</sub> and 30% 1M, gives a resultant chart for 75% 2M<sub>1</sub> and 25% 1M that can be saved and used for later comparison with the user's experimental chart. Although the WILDFIRE method has been successfully applied to younger fault rock samples, the uncertainty in determined proportion of 2M<sub>1</sub> in our samples resulted in a c. 100 Ma uncertainty in the calculated date (y-axis intercept), which is too large to be useful. An attempted application of the IAA method is shown in Figure 6a for sample GSWA 189281, for which we measured intermediate size fractions in addition to the finest fraction and a coarse fraction.

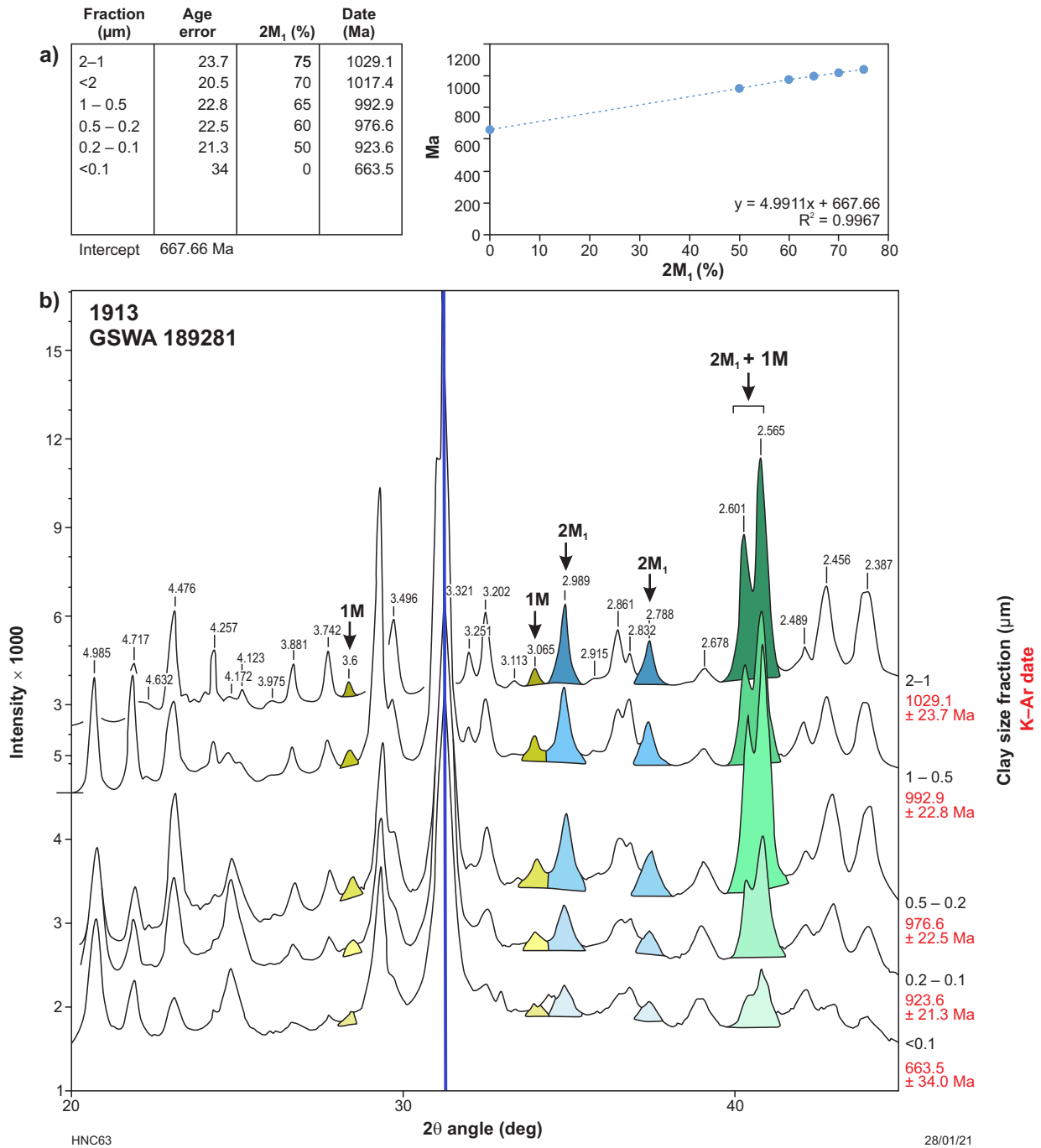


Figure 6. Illite Age Analysis (IAA) and determination of clay polymorphs for GSWA 189281: a) IAA calculation yielding an intercept age of 667.7 Ma, and an age for the <0.1  $\mu\text{m}$  size fraction of 663.5 Ma. This is a close match for this sample, and depends on an accurate determination of the proportion of  $2M_1$ , which is in practice difficult to calculate; b) comparison XRD charts for clay size fractions and clay polymorphs 1M (yellow),  $2M_1$  (blue) and the  $1M + 2M_1$  (green) combination peaks. With decrease in grain size the relative peak area of  $2M_1$  to 1M polymorphs decreases, indicating the decrease of the  $2M_1$  component (cataclastic) inherited from the host rock. A small remnant of  $2M_1$  in the <0.1  $\mu\text{m}$  size fraction represents authigenic  $2M_1$  (Grathooff and Moore, 1996; Torgersen et al., 2015). Blue line is the quartz peak

Detailed discussion by Torgersen et al. (2015) identified complications in applying the IAA and the need to consider faulting conditions, most notably temperature, and the possibility of older fault movement events. The two-part mixing model of IAA may not be valid. Elevated temperatures during a faulting event can produce authigenic  $2M_1$  as individual grains or as recrystallization rims on existing larger inherited  $2M_1$  grains (Zwingmann et al., 2010a; Lobens et al., 2011; Viola et al., 2013). The temperature of the faulting event can be identified from the illite crystallinity Kübler index (KI; Kübler, 1968). It is also possible that the larger clay fractions may contain authigenic  $2M_1$  produced by an older faulting event. To eliminate these variable influences (Torgersen et al., 2015) concluded that the date of the finest fraction (ideally  $<0.1 \mu\text{m}$ ) represents the most recent fault movement. Coarser fractions may represent mixed ages, but may provide information regarding older faulting events.

## Illite crystallinity

The illite crystallinity or KI (Kübler, 1968) was determined from  $<2 \mu\text{m}$  clay separates with XRD analyses conducted on a Bruker D4 Endeavour X-ray diffractometer (CoK $\alpha$ ), operated at 40 kV and 30 mA at a scanning rate of  $1^\circ(2\theta)/\text{min}$  and  $0.05^\circ(2\theta)/\text{step}$ . The standard measurement of KI is on the  $<2 \mu\text{m}$  size fraction. KI is defined as the width of the first-order illite basal reflection (10 Å peak) at half height and expressed in  $\Delta 2\theta$  values. KI decreases with increasing illite crystallinity, with temperature being the most important controlling factor (Fig. 7; Merriman and Frey, 1999). The KI results of this study were calibrated to the Crystallinity Index Standard (CIS) scale using the procedure and interlaboratory standards of Warr and Mählmann (2015).

## Results

### Petrography

Six representative samples were examined in standard thin sections. A sample of fault gouge (GSWA 189218) from the South Brumby Creek Fault, comprises a mosaic of recrystallized microcrystalline quartz which envelopes fine-grained fragments, streaks and bands consisting of sheared, cryptocrystalline, ferruginous clouded clay–silica material, cut by veinlets of quartz (Fig. 8a,b).

A sample of quartz–ironstone breccia (GSWA 189264) from the Mount Vernon Fault consists of angular, medium- to coarse-grained fragments of corroded and highly deformed quartz (Fig. 8c) set in a ferruginous matrix which contains pods of corroded quartz and Fe-oxide–veined quartz grains. Grains of quartz are commonly coated by iron oxide, which forms vein networks through the rock (Fig. 8d,e).

A slickenline sample (GSWA 189270) from Tonys Fault, is dominated by fragmental to sheared assemblages of recrystallized microcrystalline to fine-grained, angular to sheared, Fe-clouded quartz mosaics including clay minerals and zones of quartz mylonite (Fig. 8f,g). The mylonitic zones may be intercalated with sheared, clouded fragments of cryptocrystalline clay and quartz and include interstitial, brilliant-red goethite (Fig. 8g). Opaque Fe-oxide veins are widespread.

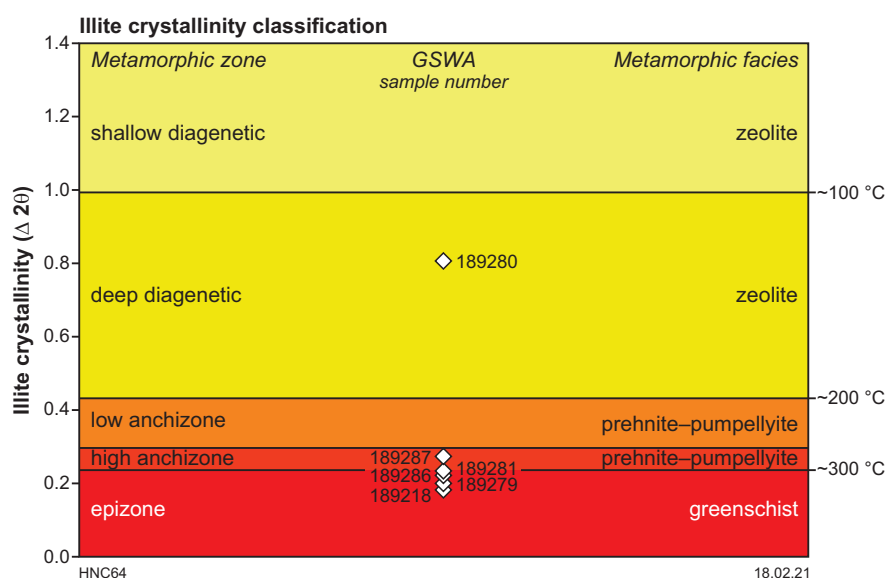


Figure 7. Illite crystallinity (Kübler Index, KI; Kübler [1968]) classification showing temperature of illite formation determined from KI with corresponding metamorphic zones and metamorphic facies, and range of GSWA samples for which KI was measured ( $<2 \mu\text{m}$  size fraction; Table 4)

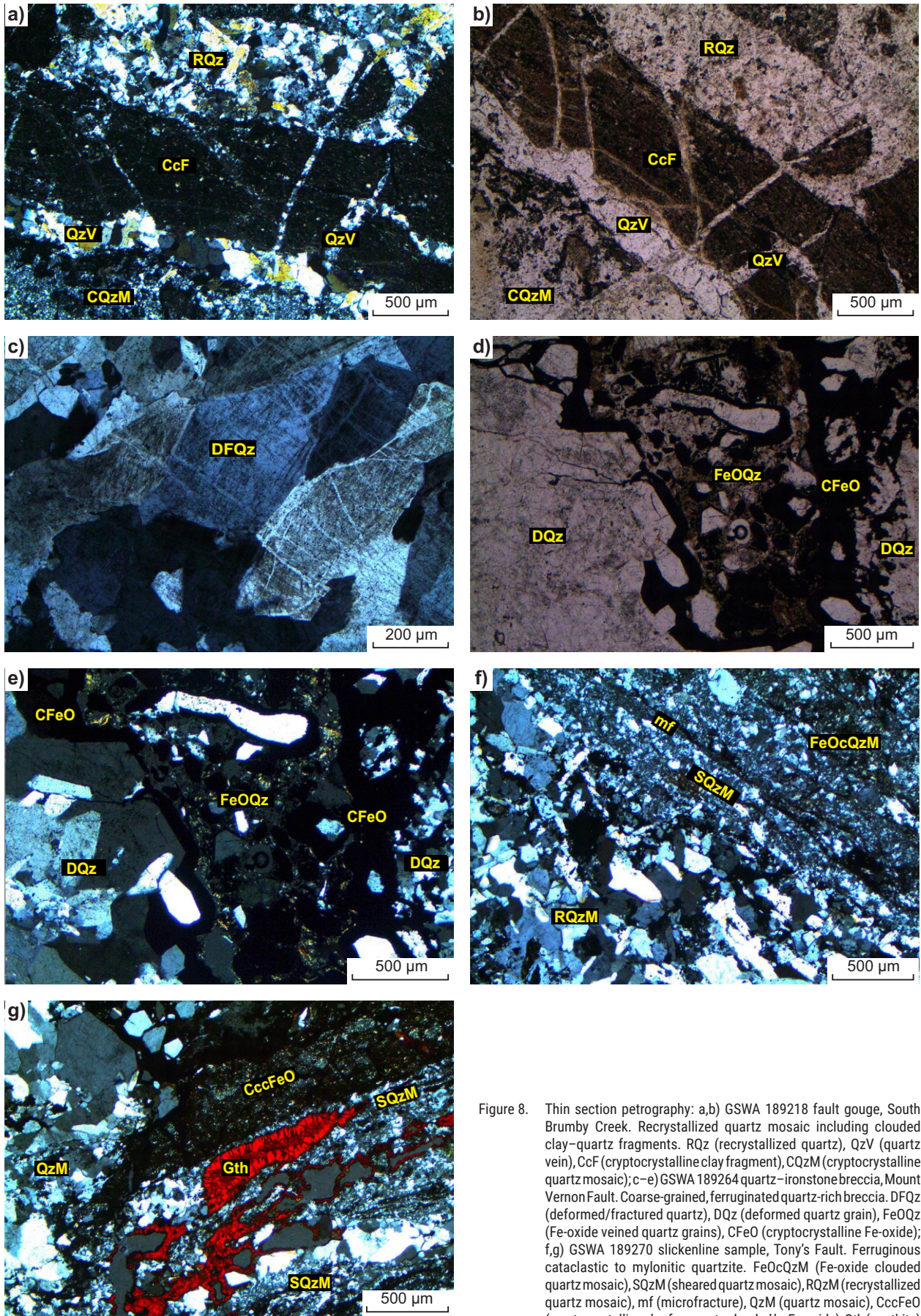


Figure 8. Thin section petrography: a,b) GSWA 189218 fault gouge, South Brumby Creek. Recrystallized quartz mosaic including clouded clay-quartz fragments. RQz (recrystallized quartz), QzV (quartz vein), CcF (cryptocrystalline clay fragment), CQzM (cryptocrystalline quartz mosaic); c-e) GSWA 189264 quartz-ironstone breccia, Mount Vernon Fault. Coarse-grained, ferruginated quartz-rich breccia. DFQz (deformed/fractured quartz), DQz (deformed quartz grain), FeOQz (Fe-oxide veined quartz grains), CFeO (cryptocrystalline Fe-oxide); f,g) GSWA 189270 slickenline sample, Tony's Fault. Ferruginous cataclastic to mylonitic quartzite. FeOcQzM (Fe-oxide clouded quartz mosaic), SQzM (sheared quartz mosaic), RQzM (recrystallized quartz mosaic), mf (microfracture), QzM (quartz mosaic), CccFeO (cryptocrystalline clay fragments clouded by Fe-oxide), Gth (goethite)

HNC68a

25/01/21

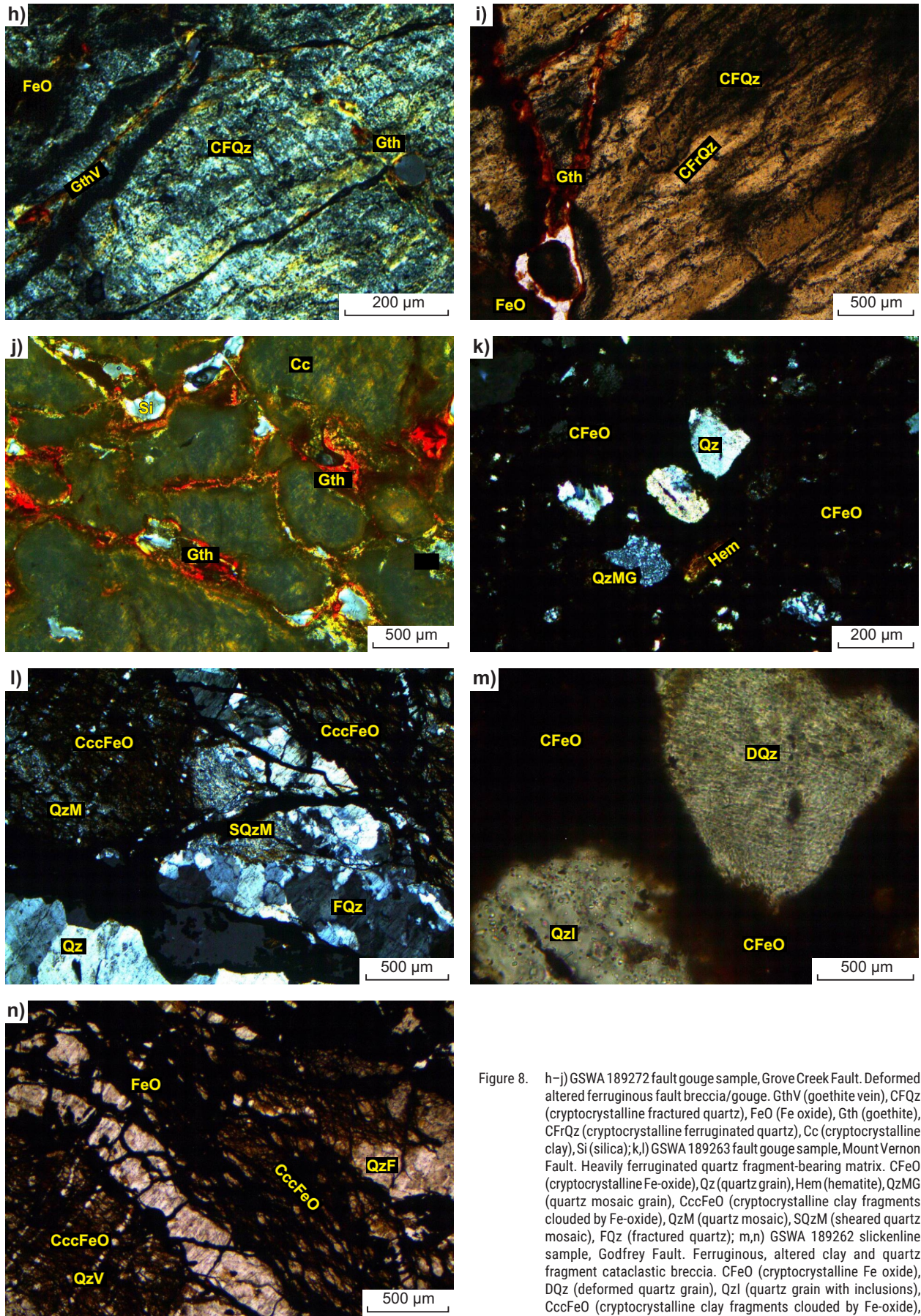


Figure 8. h-j) GSWA 189272 fault gouge sample, Grove Creek Fault. Deformed altered ferruginous fault breccia/gouge. GthV (goethite vein), CFQz (cryptocrystalline fractured quartz), FeO (Fe oxide), Gth (goethite), CFrQz (cryptocrystalline ferruginated quartz), Cc (cryptocrystalline clay), Si (silica); k,l) GSWA 189263 fault gouge sample, Mount Vernon Fault. Heavily ferruginated quartz fragment-bearing matrix. CFeO (cryptocrystalline Fe-oxide), Qz (quartz grain), Hem (hematite), QzMG (quartz mosaic grain), CccFeO (cryptocrystalline clay fragments clouded by Fe-oxide), QzM (quartz mosaic), SQzM (sheared quartz mosaic), FQz (fractured quartz); m,n) GSWA 189262 slickenline sample, Godfrey Fault. Ferruginous, altered clay and quartz fragment cataclastic breccia. CFeO (cryptocrystalline Fe oxide), DQz (deformed quartz grain), QzI (quartz grain with inclusions), CccFeO (cryptocrystalline clay fragments clouded by Fe-oxide), FeO (Fe-oxide), QzV (quartz veins), QzF (quartz fragments)

HNC68b

25/01/21

A fault gouge sample (GSWA 189272) from the Grove Creek Fault consists of coarse-grained, angular to strongly sheared fragments composed of strongly fractured and internally deformed quartz (Fig. 8h,i), and fragments composed of cryptocrystalline clay minerals injected by veins of quartz, goethite and hematite (Fig. 8j). Interstitial concretions of goethite and hematite are common, particularly in association with clay-dominated fragments (Fig. 8j).

A sample of host rock (GSWA 189263) adjacent to the Mount Vernon Fault consists of a uniform, microcrystalline assemblage of silt-size angular quartz fragments and fragments of chert (Fig. 8k) cemented by a cryptocrystalline hematite matrix. The quartz grains display corroded rims, internal deformation and an abundance of fluid inclusions (Fig. 8l). Discrete lumps and grains of hematite are present (Fig. 8k).

A slickenside sample (GSWA 189262) from near the junction of the Godfrey and Mount Vernon Faults consists of fine- to medium-grained ferruginous cryptocrystalline clay-quartz injected with veins of Fe-oxide, quartz fragments and medium-grained quartz (Fig. 8m,n).

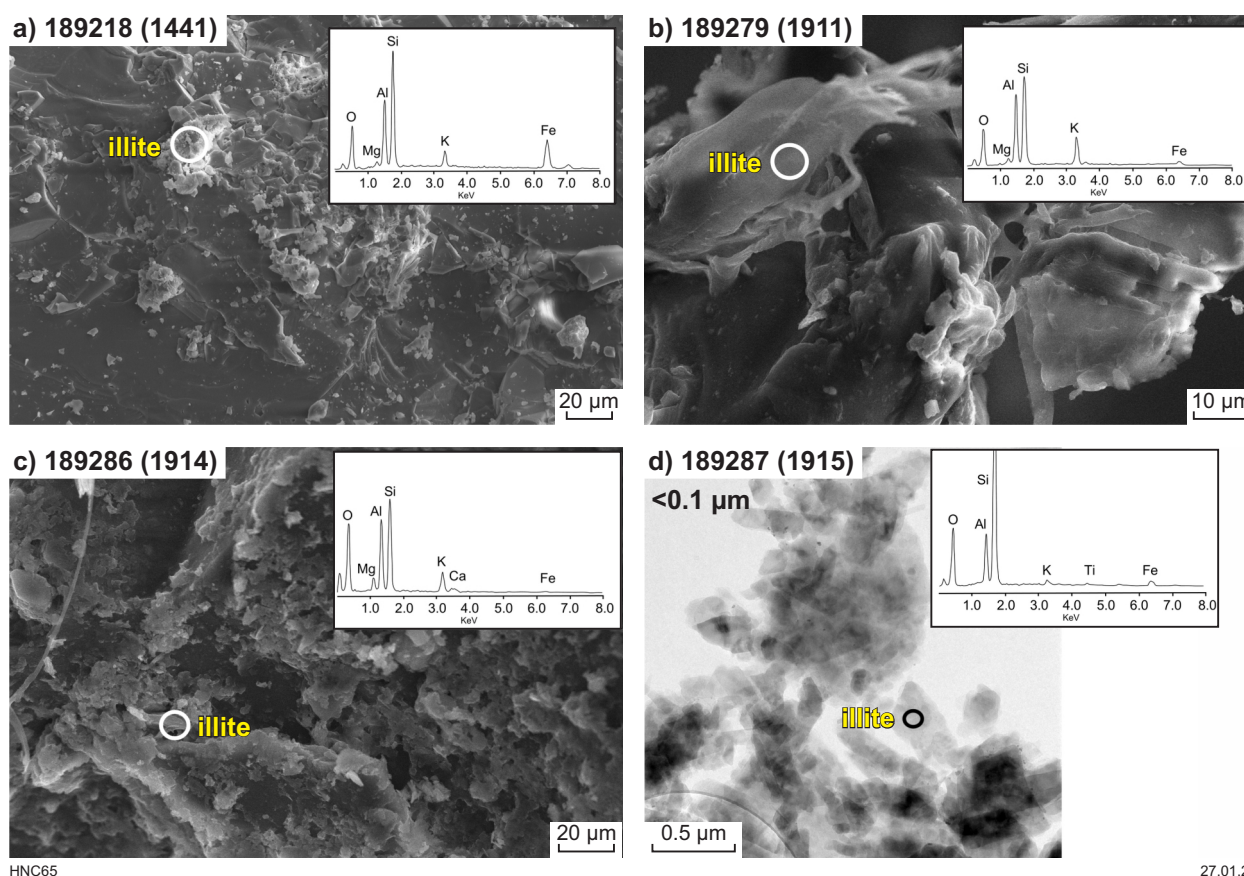
## Scanning electron microscopy (SEM)

SEM results and images of three representative samples are summarized in Figure 9. The surface of fault gouge sample GSWA 189218 (Brumby Creek Fault) consists

mainly of crushed quartz fragments with minor flakes and fibres of authigenic clay minerals (illite/muscovite) about 20–30  $\mu\text{m}$  wide (Fig. 9a). No major K-feldspar alteration or relics were identified. EDS analysis confirms the presence of K-rich clay minerals such as illite or muscovite (Si, Al, O, K peaks). The surface of sample GSWA 189279 (Six Mile Creek Fault) consists of large clusters of synkinematic minerals comprising illite (identified and confirmed by EDS analysis) and authigenic mineral components comprise platy and fibrous illite material (Fig. 9b). Authigenic illite fibres extend from platy particles up to several micrometres long. The surface of sample GSWA 189286 (Six Mile Creek Fault) shows very fine-grained platy illite particles (<5  $\mu\text{m}$ ) with authigenic illite fibres up to several micrometres long (Fig. 9c).

## Transmission electron microscopy (TEM)

TEM observations of the separated clay fractions document the occurrence of distinct groups of particles comprising idiomorphic platy and fibrous illite, together with hexagonal idiomorphic chlorite and kaolinite with well crystallized edges. A representative TEM image is shown in Figure 9d (GSWA 189287, <1  $\mu\text{m}$ , Six Mile Creek Fault, drillcore AB62, 443.72 m). Illite/muscovite was confirmed by EDS analysis with low K concentration within the particles.



HNC65

27.01.21

Figure 9. SEM and TEM images of representative samples: a) SEM image of sample GSWA 189218 (South Brumby Creek Fault gouge; cf. Figures 4c, 8a,b); b) SEM image of sample GSWA 189280 (Abra Cross Fault, core sample, 225 m depth); c) SEM image of sample GSWA 189286 (Six Mile Creek Fault, drillcore AB62, 396.7 m depth); d) TEM image of sample fraction GSWA 189287 <2  $\mu\text{m}$  (Six Mile Creek Fault, drillcore AB62, 443.72 m depth). SEM and TEM images show representative EDS spectra. Numbers in brackets are CSIRO laboratory numbers

## X-ray diffraction

XRD analysis of the whole-rock sample split (GSWA 189263) indicates the presence of quartz, goethite, illite and kaolinite as the major mineral phases (Table 3). The <2 µm clay fraction of sample GSWA 189279 comprises kaolinite as the major mineral phase with only low amounts of illite and quartz. The <2 µm clay fractions from samples GSWA 189280 and 189287 contain variable amounts of illite 2M<sub>1</sub> and 1M polytypes as the major mineral phase. In sample GSWA 189286, the main mineral component is smectite, together with only the 2M<sub>1</sub> polytype of illite and with traces of quartz, clinochlore and dolomite. All <2 µm fractions of the samples contain a variable amount of clinochlore (1MIIB polytype). The <2 µm fraction of sample GSWA 189287 also contains the clinochlore 1MIB Fe polytype. No traces of K-feldspar contamination could be identified by XRD.

## Illite crystallinity

Illite crystallinity determined from the <2 µm fraction ranges from deep diagenetic (Fig. 7), KI = 0.806 (GSWA 189280), to epizone greenschist, KI = 0.182 (GSWA 189218). A total of four samples fall in epizone greenschist and one sample in high anchizone (Fig. 7, Table 4), indicating temperatures over ~300 °C and ~250 °C respectively. At these elevated temperatures, authigenic 2M<sub>1</sub> can form in the finer fractions and as rims on the larger, inherited 2M<sub>1</sub> grains present in intermediate clay size fractions (Torgersen et al., 2015).

## K–Ar dating

K–Ar analytical data are shown in Tables 5 and 6. The ages of one whole-rock (WR) and 20 clay fractions range from 1506.6 ± 30.2 Ma for sample GSWA 189263 (WR date of country rock adjacent to the Mt Vernon Fault) to 238.1 ± 5.6 Ma for sample GSWA 189279 (lithified fault gouge from drillcore AB62, Six Mile Creek Fault; Fig. 3, Table 6). Concentrations of K<sub>2</sub>O in the clay fractions range from 0.55% for sample GSWA 189265 (0.2 – 2.0 µm; Brumby Creek Fault) to a high of 6.52% for sample GSWA 189280 (<2 µm; AB60a, Abra Cross Fault). Variable K<sub>2</sub>O concentration in the WR and clay size fractions is caused by mixtures with other mineral phases, such as kaolinite and goethite (Table 3). The K<sub>2</sub>O concentration for the WR split is low at 1.28%, for sample GSWA 189263, supporting XRD and SEM observations that indicate illite/muscovite are the only K-bearing phases (Table 5). Radiogenic <sup>40</sup>Ar content ranges from 73.9 to 99.5%, indicating reliable analytical conditions for all analyses with no significant atmospheric <sup>40</sup>Ar contamination despite the very low K<sub>2</sub>O concentration of WR split GSWA 189263. As noted in the sample preparation section, the degree of silicification and quartz content placed some constraints on the analysis of the fault rock samples. Where little material was obtained from separated fractions, it was combined within a broader size fraction range for dating or further analysis.

**Table 3. XRD data**

GSWA sample ID	Whole rock ID	Quartz (%)	Kaolinite (%)	Illite (%)	Goethite (%)	Hematite (%)	Anatase (%)	Rutile (%)	Calcite (%)	Alunite (%)	
189263	1635	50–55	2–5	7–12	30–35		1–2	traces			
	Clay fractions	Quartz (%)	Kaolinite (%)	Illite/mica 2M1 (%)	Illite/mica 1M (%)	Goethite (%)	Smectite (%)	Clinochlore 1MIIB (%)	Clinochlore 1MIB Fe (%)	Rutile (%)	Dolomite/ankerite (%)
	(<2µm)										
189279	1911	1	90	6				3		traces	
189280	1912	2		47	33	4		14		traces	
189281	1913	5		48	30	4		13		1	
189286	1914	4		20			69	4			4
189287	1915	traces		52	24			11	12	1	
210013	2252	ND	ND	ND	ND	ND	ND	ND	ND	ND	ND
189265	1637	ND	ND	ND	ND	ND	ND	ND	ND	ND	ND

Note: ND, not determined

**Table 4. Illite crystallinity (KI)**

GSWA sample ID	CSIRO sample ID	Size fraction (µm)	KI	Zone
189218	1441	<2	0.18234	Epizone greenschist
189279	1911	<2	0.20005	Epizone greenschist
189280	1912	<2	0.80649	Deep diagenetic
189281	1913	<2	0.23412	Epizone greenschist
189286	1914	<2	0.22186	Epizone greenschist
189287	1915	<2	0.27364	High anchizone

Table 5. K–Ar data

Location	Sample type Whole rock WR or micron	K <sub>2</sub> O (%)	Radiogenic <sup>40</sup> Ar (mol/g)	Radiogenic <sup>40</sup> Ar (%)	Age (Ma)	Error (Ma)	Time scale (Gradstein et al., 2004)
<b>Mount Vernon Fault System</b>							
Brumby Creek Fault - FG	189218; 0.2 – 0.1 µm	0.930	2.568E-09	96.5	1141.4*	58.6	Mesoproterozoic (Stenian)
Brumby Creek Fault - FG	189218; 2–1 µm	0.556	1.529E-09	96.1	1137.9*	26.2	Mesoproterozoic (Stenian)
Brumby Creek Fault - FG	189265; <0.2 µm	1.25	2.479E-09	73.9	885.5*	45.9	Neoproterozoic (Tonian)
Brumby Creek Fault - FG	189265; 2 – 0.2 µm	0.546	1.944E-09	98.1	1370.6	31.6	Mesoproterozoic (Ectasian)
Mount Vernon Fault - WR	189263	1.28	5.23E09	98.8	1506.6	30.2	Mesoproterozoic (Calymmian)
<b>Quartzite Well Fault System</b>							
Quartzite Well Fault - FG	210013; <0.5 µm	1.05	1.941E-09	92.1	837.6*	43.0	Neoproterozoic (Tonian)
Quartzite Well Fault - FG	210013; 2–1 µm	0.630	1.335E-09	93.7	932.7	21.6	Neoproterozoic (Tonian)
Six Mile Creek Fault - FG	189279-AB62-150 m; <0.1 µm	0.677	2.989E-10	82.7	238.1*	5.6	Middle Triassic (Anisian)
Six Mile Creek Fault - FG	189279-AB62-150 m; 2–1 µm	1.09	2.261E-09	98.9	917.5	21.1	Neoproterozoic (Tonian)
Six Mile Creek Fault - FG	189286-AB62-396.7 m; <0.1 µm	1.85	1.224E-09	77.6	346.1*	8.1	Carboniferous – Lower Mississippian (Tournaisian)
Six Mile Creek Fault - FG	189286-AB62-396.7 m; <2 µm	1.10	2.165E-09	90.22	880.2*	17.9	Neoproterozoic (Tonian)
Six Mile Creek Fault - FG	189287-AB62-443.72 m; <0.1 µm	4.37	7.708E-09	98.5	806.5*	16.2	Neoproterozoic (Cryogenian)
Six Mile Creek Fault - FG	189287-AB62-443.72 m; <0.4 µm	5.16	9.458E-09	98.8	831.8*	16.9	Neoproterozoic (Cryogenian)
Six Mile Creek Fault - FG	189287-AB62-443.72 m; 6–2 µm	5.53	1.447E-08	99.5	1096.5	22.1	Mesoproterozoic (Stenian)
Abra Cross Fault - FG	189281-AB60a-216.8 m; <0.1 µm	6.36	8.846E-09	98.2	663.5*	34.0	Neoproterozoic (Cryogenian)
Abra Cross Fault - FG	189281-AB60a-216.8 m; 0.2 – 0.1 µm	5.69	1.190E-08	98.9	923.6	21.3	Neoproterozoic (Tonian)
Abra Cross Fault - FG	189281-AB60a-216.8 m; 0.5 – 0.2 µm	5.98	1.344E-08	99.1	976.6	22.5	Neoproterozoic (Tonian)
Abra Cross Fault - FG	189281-AB60a-216.8 m; 1 – 0.5 µm	6.06	1.392E-08	99.5	992.9	22.8	Neoproterozoic (Tonian)
Abra Cross Fault - FG	189281-AB60a-216.8 m; 2–1 µm	5.86	1.410E-08	99.5	1029.1	23.7	Mesoproterozoic (Stenian)
Abra Cross Fault - FG	189280-AB60a-225 m; 1 to <0.1 µm	4.40	7.476E-09	98.0	782.2*	40.1	Neoproterozoic (Cryogenian)
Abra Cross Fault - FG	189280-AB60a-225 m; <2 µm	6.52	1.456E-08	99.5	971.9	19.5	Neoproterozoic (Tonian)

NOTE: \* indicates fault movement date. Abbreviations: FG, fault gouge; WR, whole rock

Table 6. K–Ar dates and tectonic events

GSWA sample ID	CSIRO sample ID	Sample type	Fault name Dip and dip direction	Sense of movement	Host rock formation and stratigraphic level	Sample recovery	Depth	Location (Zone 50) Easting Northing	Size fraction (µm)	Date and uncertainty (Ma)	Tectonic event
<b>MOUNT VERNON FAULT SYSTEM</b>											
189265	1637	FG	North Brumby Creek Fault 45° to 355°	reverse 20 cm	Kiangi Creek base	exposed	surface	679113 7314768	2 – 0.2 <0.2	1370 ± 31.6 885.5 ± 45.9	MD Kuparr Event
189218	1441	FG	South Brumby Creek Fault 35° 230°	reverse 25 cm	Kiangi Creek base	exposed	surface	679113 7314768	2–1 0.2 – 0.1	1137.9 ± 26.2 1141.4 ± 58.6	Mutherbukin Event Mutherbukin Event
189263	1635	SHR	Mount Vernon Fault steep to south	probable normal	Kiangi Creek base	exposed	surface	615826 7312052	WR	1506.6 ± 30.2	Basin forming event, coeval with deposition
<b>QUARTZITE WELL FAULT SYSTEM</b>											
210013	2252	FG	Quartzite Well Fault, NA	probable reverse	Kiangi Creek mid	exposed	surface	639014 7274546	2–1 <0.5	932.7 ± 21.6 837.6 ± 43.0	MD Kuparr Event
189279	1911	FG	Six Mile Creek Fault, NA	probable reverse	Kiangi Creek mid	drillcore AB62	150 m	662148 7274152	2–1 <0.1	917.5 ± 21.1 238.1 ± 5.6	MD New fault movement
189286	1914	FG	Six Mile Creek Fault, NA	probable reverse	Kiangi Creek mid	drillcore AB62	396.7 m	662148 7274152	<2 <0.1	880.2 ± 17.9 346.1 ± 8.1	Kuparr Event New fault movement
189287	1915	FG	Six Mile Creek Fault, NA	probable reverse	Kiangi Creek mid	drillcore AB62	443.7 m	662148 7274152	6–2 0.4 <0.1	1096.5 ± 22.1 831.8 ± 16.9 806.5 ± 16.2	MD Kuparr Event Kuparr Event
189281	1913	FG	Abra Cross Fault, NA	probable reverse	Kiangi Creek mid	drillcore AB60a	216.8 m	660475 7273597	2–1 1 – 0.5 0.5 – 0.2 0.2 – 0.1 <0.1	1029.1 ± 23.7 992.9 ± 22.8 976.6 ± 22.5 923.6 ± 21.3 663.5 ± 34.0	MD MD MD MD New fault movement
189280	1912	FG	Abra Cross Fault, NA	probable reverse	Kiangi Creek mid	drillcore AB60a	225 m	660475 7273597	<2 1 to <0.1	971 ± 19.5 782 ± 40.1	MD Kuparr Event

Abbreviations: FG, fault gouge; SHR, sheared host rock; MD, coarser fraction mixed date; NA, dip and dip direction not available

All dated samples show a progressive reduction in age with decreasing grain size. A total of five size fractions dated for sample GSWA 189281 show this inclined age spectrum (Fig. 6, Tables 5 and 6). Following the method of Torgersen et al. (2015), the finest (ideally <0.1 µm) size fraction is considered to date authigenic illite predominantly  $1M/1M_d$ . Any  $2M_1$  present is also considered authigenic given the KI indication of elevated temperature. The date determined for the <0.1 µm fraction is therefore interpreted as the age of the most recent fault movement. Coarser size fractions represent mixed ages as these coarser fractions contain remnants of  $2M_1$  illite/muscovite which may be inherited or detrital, or which formed during a previous high-temperature metamorphic or faulting event. Dating of sample 189287 shows that, although the <0.4 µm fraction is older ( $831.8 \pm 16.9$  Ma) than the finest (<0.1 µm) fraction ( $806.5 \pm 16.2$  Ma), these dates are within uncertainty of each other. This demonstrates that where a <0.1 µm fraction cannot be obtained, slightly coarser grain sizes may provide valid indications of the timing of fault movement.

### Mount Vernon Fault system

Individual strands of the Mount Vernon Fault system revealed different dates, indicating that fault movement occurred on different strands at different times rather than the whole fault system rupturing during a single faulting event.

Sample GSWA 189265 on the North Brumby Creek Fault returned dates of  $1370.6 \pm 31.6$  Ma (0.2 – 2.0 µm) and  $885.5 \pm 45.9$  Ma (<0.2 µm). The date for the <0.2 µm fraction is interpreted as the age of the most recent phase of fault movement on this fault. This resulted in authigenic illite growth (and possible resetting of existing illite/muscovite, if present, either from an older faulting event or from inherited grains).

Sample GSWA 189218 from the South Brumby Creek Fault yielded dates of  $1141.4 \pm 58.6$  Ma (0.1 – 0.2 µm) and  $1137.9 \pm 26.2$  Ma (1–2 µm), both within uncertainty of each other (Fig. 3, Table 6). This is interpreted to indicate complete resetting of existing illite in the coarser size fraction, as well as new illite growth during the last fault movement phase. The  $1141.4 \pm 58.6$  Ma date of the finest fraction (0.1 – 0.2 µm) is adopted as the age of the most recent fault movement on this fault strand. This result is within uncertainty of the youngest constraints for the Mutherbukin Tectonic Event (Johnson et al., 2011b; Korhonen et al., 2015, 2017). This fault strand was not reactivated by the younger brittle event at  $885.5 \pm 45.9$  Ma which took place on the nearby fault strand (GSWA 189265, North Brumby Creek Fault).

Sample GSWA 189263 yielded a whole-rock date of  $1506.6 \pm 30.2$  Ma for fine-grained sandstone of the Kiangi Creek Formation. The age of deposition of the Kiangi Creek Formation has been constrained by SHRIMP U–Pb dating of zircon and xenotime at 1590–1514 Ma (Zi et al., 2015). The K–Ar date of  $1506.6 \pm 30.2$  Ma obtained for the whole rock is within uncertainty of that obtained for the timing of deposition. If the  $2M_1$  illite/muscovite is detrital, it might be expected to give a spread of dates, or an average of dates, indicative of the age range of the source rocks of the sandstone. The coincidence of the obtained date with the timing of deposition, may suggest a diagenetic origin related

to burial and compaction in the basin. However, growth of  $2M_1$  illite/muscovite requires temperatures in excess of 200 °C, the transition between diagenesis and low-grade metamorphism, which is not evident in the sedimentary rocks of the Edmund Group (Cutten et al., 2016). The  $1506.6 \pm 30.2$  Ma K–Ar date might instead record an episode of normal faulting, and fault-controlled hydrothermal fluid flux, associated with ongoing basin subsidence and deposition of the Kiangi Creek Formation.

### Quartzite Well Fault system

Fault rocks were recovered by from three localities on the Quartzite Well Fault and branch faults, as well as from drillcore which intersected two southern fault strands of the system, the Six Mile Creek Fault (drillhole AB62) and the Abra Cross Fault (drillhole AB60a).

From the main Quartzite Well Fault, two clay fractions in GSWA 210013 returned dates of  $932.7 \pm 21.6$  Ma (1–2 µm) and  $837.6 \pm 43.0$  Ma (<0.5 µm). The finer fraction (<0.5 µm) is considered to date the most recent movement on this fault strand. A slickenside sample from the Tonys Fault (GSWA 189270), and a fault gouge sample from the Grove Creek Fault (GSWA 189272) both proved unsuitable for K–Ar dating because they are too silicified.

Three samples of lithified fault gouge were recovered from drillcore AB62, which intersected the Six Mile Creek Fault 500 m south of the Quartzite Well Fault (Fig. 3c). From GSWA 189279 (150 m depth), two fractions were dated at  $917.5 \pm 21.1$  Ma (1–2 µm) and  $238.1 \pm 5.6$  Ma (<0.1 µm). The finest fraction with the younger date of  $238.1 \pm 5.6$  Ma indicates previously undocumented Triassic fault movement. From GSWA 189286 (depth 396.7 m), two fractions were dated at  $880.2 \pm 17.9$  Ma (<2 µm) and  $346.1 \pm 8.1$  Ma (<0.1 µm). The finest fraction with the younger date of c. 346 Ma reveals previously undocumented Carboniferous fault activity. From GSWA 189287 (depth 443.7 m), three fractions were dated at  $1096.5 \pm 22.1$  Ma (2–6 µm),  $831.8 \pm 16.9$  Ma (0.4 µm) and  $806.5 \pm 16.2$  Ma (<0.1 µm). The dates for the 0.4 and <0.1 µm fractions are within uncertainty of each other, and are considered to date the most recent movement on this fault strand.

Two samples of lithified fault gouge were recovered from drillhole AB60a which intersects the Abra Cross Fault. The drillhole is at a location 1100 m south of the Quartzite Well Fault and 1500 m southwest of drillhole AB62. From GSWA 189281 (216.8 m depth), five fractions (Fig. 6) were dated at  $1029.1 \pm 23.7$  Ma (1–2 µm),  $992.9 \pm 22.8$  Ma (0.5 – 1.0 µm),  $976.6 \pm 22.5$  Ma (0.2 – 0.5 µm),  $923.6 \pm 21.3$  Ma (0.1 – 0.2 µm), and  $663.5 \pm 34.0$  Ma (<0.1 µm). For this sample, application of the IAA method appears to be successful, with an intercept age of 667.65 Ma which is within uncertainty of the c. 663.5 Ma date for the finest fraction (Fig. 6a). However, the validity of the IAA date rests on the calculation of polytype percentages which, in practice, have large uncertainties. The finest fraction, with a date of c. 663 Ma, reveals a previously undocumented Neoproterozoic fault movement event in the Capricorn Orogen. From GSWA 189280 (225 m depth), two fractions were dated at  $971.8 \pm 19.5$  Ma (<2 µm) and  $782.5 \pm 40.1$  Ma (<0.1 – 1.0 µm). The date obtained for the finest fraction is considered to record the most recent movement on this fault strand.

## Discussion

The K–Ar dating method has previously been applied to dating fault movements in Phanerozoic rocks (Zwingmann et al., 2004; Torgersen et al., 2015), and this study is one of the first to successfully apply the technique to faulting in much older, Proterozoic rocks (cf. Viola et al., 2013; Uysal et al., 2020). The study also allows differentiation of successive fault movement events on separate fault strands within a single fault system, as well as possibly identifying multiple faulting events on a single fault strand. Obtaining detailed fault kinematic data has been severely limited due to the rarity of surface fault rock exposure. The methods applied in this study would be more powerful had these data been available in the field and more favourable future studies could potentially distinguish faults of different kinematic significance, providing greater understanding of the tectonic history of the cover basins.

In the medium- to high-grade basement rocks of the Capricorn Orogen, the tectonic and magmatic history has been well studied, and the timing of events well constrained – largely by application of U–Pb dating of zircon, baddeleyite, xenotime and monazite (Sheppard et al., 2005, 2010; Johnson et al., 2011b). Constraining the age of faulting and folding in the overlying sedimentary rocks of the Edmund and Collier Groups is significantly more difficult because these events occurred at low temperatures that were insufficient for the growth or resetting of most common mineral chronometers. Illite crystallinity values (KI; Kübler, 1968), determined from fault rock <2 µm clay fractions, indicate that temperature conditions of faulting were between ~250 and 300 °C (Table 4), although the sedimentary rocks themselves indicate that regional basin temperatures did not exceed 200 °C (Cutten et al., 2016). Previous constraints on the timing of deformation of the Edmund and Collier Basins are relatively broad and derived principally from indirect or crosscutting relationships, such as the age of detrital zircons or the age of emplacement of deformed and undeformed dolerite dykes and sills. Direct dating of the brittle faulting events is critical for the determination of the absolute timing and distribution of tectono-thermal events in these overlying basins.

XRD diffraction charts of clay size fractions from 2 µm to <0.1 µm show, by decreasing peak area, successively decreasing percentage of 2M<sub>1</sub> illite polytype with finer diminishing grain size (Fig. 6). K–Ar dates obtained from intermediate size fractions are interpreted to indicate mixed ages. The application of the IAA method and determination of percentage of 2M<sub>1</sub> using the formula of Grathooff and Moore (1996), and WILDFIRE software gave incoherent results, interpreted as due to the failure of the assumption that all 2M<sub>1</sub> is inherited detrital or wallrock illite/muscovite contamination. K–Ar results generally do show inclined age spectra with grain size, thus intermediate size fractions are recording mixed ages, but for possible additional reasons. Because faulting occurred at temperatures >250 °C, there is the likelihood of new authigenic 2M<sub>1</sub> which is indistinguishable from inherited 2M<sub>1</sub>. However, in the finest size fractions (ideally <0.1 µm), inherited 2M<sub>1</sub> percentage is expected to be close to zero, as applications in other studies have demonstrated. Thus, the illite in these finer fractions is considered to be authigenic and the returned K–Ar dates represent the ages of most recent fault movement. Most of these define newly identified early Neoproterozoic to

Paleozoic events, most notably the 885–782 Ma Kuparr Tectonic Event (Cutten and Johnson, 2018).

## Kuparr Tectonic Event

Four samples in this study yielded K–Ar dates from the finer fractions within the 885–782 Ma age range one associated with the Mount Vernon Fault system, and three within the Quartzite Well Fault system (Fig. 10). These K–Ar dates constrain the timing of faulting in the upper crust and, together with other previously published dates, define the age of the 885–782 Ma Kuparr Tectonic Event (Cutten and Johnson, 2018). One sample (GSWA 189286) also returned a date of  $880 \pm 17.9$  Ma for the <2 µm size fraction, in addition to a date of  $346.1 \pm 8.1$  Ma for the <0.1 µm size fraction. Whereas the coarse size fractions of all other samples returned dates older than c. 917 Ma that suggest inherited detrital or included wallrock illite/muscovite 2M<sub>1</sub>, this sample (GSWA 189286) suggests a significant component of authigenic 2M<sub>1</sub> formed during the Kuparr Tectonic Event. This sample demonstrates how a single sample might identify more than one faulting event, as proposed by Torgersen et al. (2015).

Previously published dates, which are broadly coincident with the age of the Kuparr Tectonic Event, include poorly constrained <sup>40</sup>Ar/<sup>39</sup>Ar dates of 960–820 Ma (Occhipinti, 2007) from the southern Capricorn Orogen. These were interpreted to represent the timing of cooling of mid- to lower-crustal rocks as they were progressively exhumed. Similar ages (920–830 Ma) were reported from <sup>40</sup>Ar/<sup>39</sup>Ar dating of mica and SHRIMP U–Pb dating of xenotime from shear zones in basement rocks across the Gascoyne Province (Piechocka et al., 2018). These were interpreted to represent a period of Neoproterozoic shear zone reactivation resulting in exhumation of the southern part of the Capricorn Orogen and dextral strike-slip fault movement in the northern part of the orogen. U–Pb rutile dates of  $913 \pm 9$ ,  $900 \pm 8$  and  $873 \pm 8$  Ma, and additional published geochronology from basement rocks across the Capricorn Orogen (Olierook et al., 2019), were used to describe a period of northwest–southeast fault reactivation accompanied by very low- to low-grade metamorphism, abundant metasomatism, and minor leucocratic and pegmatitic magmatism between c. 955 and 830 Ma.

The 885–782 Ma Kuparr Tectonic Event may correlate with large-scale bimodal magmatism and associated mafic dyke swarms that preceded the breakup of the supercontinent Rodinia (Johnson et al., 2007; Li et al., 2008; Howell et al., 2017). In south-central Australia, the Gairdner Dyke Swarm of the plume-related Neoproterozoic Willouran large igneous province was dated at  $827 \pm 6$  Ma (Wingate et al., 1998), and the Little Broken Hill gabbro was emplaced during extension in the Willyama Inlier at  $827 \pm 9$  Ma. Slightly older dates, from syntectonic illite as young as  $905 \pm 21$  Ma from the Millungera Basin, identify previously unrecorded late Mesoproterozoic and early Neoproterozoic tectonic events in north-central Australia (Uysal et al., 2020). A comparison of paleomagnetic apparent polar wander paths (APWP) suggests that Australia, South China and Laurentia were joined during the 829–800 Ma period within the ‘Missing Link’ Rodinia construction model of Li et al. (2008). There is also evidence for a plume centre and mafic magmatism in South China at c. 825 and 780 Ma.

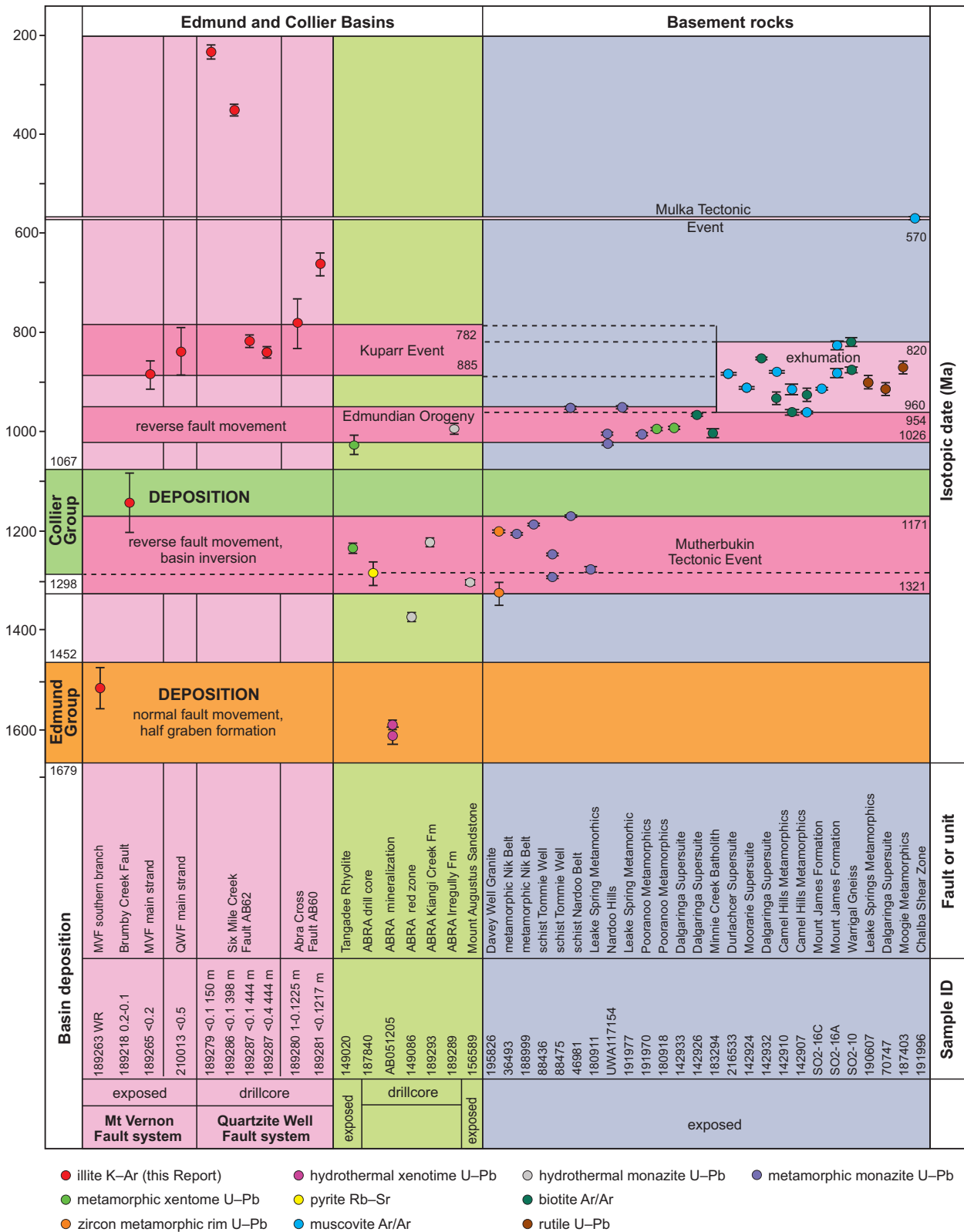


Figure 10. Ages for tectonic events, based on published U–Pb and Ar/Ar dates for basement rocks, and K–Ar dates (this study) for fault rocks. K–Ar dates from this study show the near overlap of the 885–782 Ma Kuparr Tectonic Event and a 960–820 Ma (Ar/Ar) exhumation event, as well as recent additional muscovite and biotite Ar/Ar dates and U–Pb rutile dates. The c. 1506 Ma K–Ar date is coeval with the age of deposition of the host Kiangi Creek Formation and may represent normal fault movement during the basin-forming event. The c. 1141 Ma K–Ar date records reverse movement on the Mount Vernon Fault system during the Mutherbukin Tectonic Event. Three younger K–Ar dates, at c. 663, 346 and 238 Ma, are previously unrecognized in the Capricorn Orogen

HNC66a

17.02.21

Elsewhere, in southern Africa the Zambezi Supracrustal Sequence has been dated at 880–820 Ma (Johnson et al., 2007) and the Munalu Intrusive Complex dated at 862–857 Ma (Howell et al., 2017). Although this area was likely distant from Australia and southern China at this time, these also have been interpreted as rift-related events during the initial stages of the breakup of Rodinia. Similar interpretations relating the Kuparr Event to precursors of the breakup of Rodinia were presented by Olierook et al. (2019). Although the sense of movement, which would directly indicate an extensional or compressional tectonic environment, has not been identified in this study, application of additional techniques could resolve this. However, as noted above, Piechocka et al. (2018) suggested dextral transcurrent fault movement in basement rocks at this time, and Olierook et al. (2019) also discussed strike-slip reactivation. Well-defined slickenlines, which indicate the sense of movement on visible fault-plane surfaces in the overlying basins, when coupled with direct dating of fault movement, would provide a more complete assessment of the local tectonic environment at this time. U–Pb dating of calcite associated with calcareous slickenfibres (Roberts and Walker, 2016; Mottram et al., 2020) could make this possible, and will be investigated by further study.

## Neoproterozoic and Phanerozoic dates

Three K–Ar illite dates, at c. 663, 346 and 238 Ma (Fig. 10, Table 6) from lithified fault gouge in drillcore near the Abra deposit, are considerably younger than the majority of those determined in this study and do not coincide with known events in the Capricorn Orogen. However, the  $663.5 \pm 34.0$  Ma date ( $<0.1 \mu\text{m}$  fraction; GSWA 189281) lies within the age range of the Miles Orogeny (650–600 Ma) that deformed early Neoproterozoic rocks in northwest Western Australia, as well as within the range of the earliest phases of the Paterson, Wunaamin Miliwundi (formerly King Leopold) and Petermann Orogenies (630–520 Ma) in northern and central Western Australia. The driver for these events is currently unknown. The Petermann Orogeny in central Australia was an amagmatic intracontinental transpressional event considered to have reactivated the boundary between the North, South and West Australia Cratons (Quentin de Gromard et al., 2019). Movement at c. 630 Ma on the Woodroffe Thrust in the Musgrave Province was followed by continuous cooling and exhumation of the hinterland and core of the orogen (Aitken et al., 2019; Quentin de Gromard et al., 2019). Reactivation is also recorded at about 440–400 and 200 Ma. Local modern-day activity is indicated by a 2016 magnitude  $M_L$  6 earthquake under compressive stress on a rupture plane intersecting the Woodroffe Thrust (Quentin de Gromard et al., 2019; Attanayake et al., 2020). This is considered to have resulted from in-plate horizontal stress transmission from the current convergent plate margin 2000–2500 km to the north where the Australian plate subducts beneath the Banda Arc (Quentin de Gromard et al., 2019).

The early Carboniferous  $346.1 \pm 8.1$  Ma date ( $<0.1 \mu\text{m}$  fraction; GSWA 189286) lies within a protracted series of events collectively referred to as the 450–295 Ma Alice Springs Orogeny (Haines et al., 2001) in central Australia. Initial uplift of the southeast Arunta Inlier at c. 400 Ma (Dunlap and Tessier, 1995) was followed by a second phase of uplift at c. 355 Ma (Braun et al., 1991). The latter

event was attributed to the north-trending Lasseter Shear Zone, which divides the former Neoproterozoic Centralian Superbasin, with north–south shortening to the east and coeval extension in the west in the Canning Basin, the western Officer Basin and elsewhere in Western Australia. The most significant event in the Canning Basin around this time was the mid-Carboniferous Meda Transpression (Shaw et al., 1995). Much of the dating of the intracratonic events in central Australia is ‘external’, as described by Haines et al. (2001), meaning that the identification of orogenic events was based on depositional patterns of sedimentary basins that form as foreland basins adjacent to areas of uplifted basement. This external dating is most notably by biostratigraphic methods. A complication is that a lack of coarse detritus may be as much a reflection of a very dry climate as an indicator of a lack of significant tectonic relief. However, combining information from both external and internal (direct isotopic) dating provides the most complete picture of the timing and duration of orogenic events.

The Middle to Late Triassic  $238.1 \pm 5.6$  Ma date, ( $<0.1 \mu\text{m}$  fraction; GSWA 189279) coincides with the Triassic–Jurassic Fitzroy Transpression deduced from a major unconformity across the Canning Basin, and with volcanism in the Roebuck Basin (MacNeill et al., 2018). This volcanism has been attributed to the development of a triple junction in the Early–Middle Triassic (McNeil et al., 2018) and dated at  $224.19 \pm 2.95$  Ma ( $^{40}\text{Ar}/^{39}\text{Ar}$ ) from sills within the Sapphire Graben (Mory et al., 2017). The Fitzroy Transpression refers to compressional strike slip on the eastern arm of the proposed Roebuck failed triple junction (MacNeill et al., 2018). This model is based on large-scale geometries within the Triassic seismic section interpreted to define a complex of lava deltas. Gravity and magnetic data support an apparent thickness of the volcanic complex up to 10 km (MacNeill et al., 2018). The triple junction was initiated by a magma plume which was responsible for this outpouring of flood basalts. The Neoproterozoic to Paleozoic dates identified in this study may indicate distant tectonic activity to the north and east but would require a much larger dataset to draw meaningful conclusions.

## Conclusions

The methods described here demonstrate a substantial advance towards understanding the tectonic development and deformation of Proterozoic and younger sedimentary basins. Critical to the usefulness of the K–Ar dating method is an assessment of the illite polytypes. Illite in the  $<0.1 \mu\text{m}$  fraction of our dated samples is interpreted to be authigenic, and hence can be interpreted as the age of fault movement. However, if regional metamorphism, with temperatures above 250–300 °C post-dates fault movement, then any older fault movement dates will be overprinted by metamorphic illite/muscovite. Interpretation becomes more difficult when temperatures are close to the transition from diagenesis and metamorphism ( $>200$  °C). Regional metamorphism in this temperature range can be identified from illite crystallinity of a separated  $<2 \mu\text{m}$  fraction. Samples should be collected from the fault host rocks and ideally a broader local area or a basin-wide transect.

Although K–Ar methods can date faulting events directly, they do not identify the associated tectonic setting, whether compressional, extensional or transcurrent. Slickenlines

on fault surfaces in the Proterozoic rocks described in this report may be silicified and could be described as slickenfibres, but are unsuitable for K–Ar dating, unlike the fault gouges sampled here. However, determining both the kinematics and movement history of a fault may be possible by the application of U–Pb dating of calcite slickenfibres, if these are present (Ring and Gerdes, 2016; Mottram et al., 2020), and warrants further research of faulting in Proterozoic strata.

## Acknowledgements

Mark Raven and Michael Verrall, CSIRO, are thanked for technical assistance during the course of the study.

## References

- Aitken, ARA, Quentin de Gromard, R, Joly, A, Howard, HM and Smithies, RH 2019, Thermal, rheological and kinematic conditions for channelized lower crustal flow in a threshold example: *Tectonophysics*, v. 753, p. 63–78, doi:10.1016/j.tecto.2019.01.002.
- Attanayake, J, King, TR, Quigley, MC, Gibson, G, Clark, D, Jones, A, Brennand, SL and Sandiford, M 2020, Rupture characteristics and bedrock structural control of the 2016  $M_w$  6.0 intraplate earthquake in the Petermann Ranges, Australia: *Bulletin of the Seismological Society of America*, v. 110, no. 3, p. 1037–1045, doi:10.1785/0120190266.
- Babaahmadi, A, Uysal, IT and Rossman, G 2019, Late Jurassic intraplate faulting in eastern Australia: a link to subduction in eastern Gondwana and plate tectonic reorganisation: *Gondwana Research*, v. 66, p. 1–12.
- Blay, OA, Johnson, SP, Wingate, MTD, Thorne, AM, Kirkland, CL, Tesselina, SG and Cutten, HN 2018, A new Mesoproterozoic mafic intrusive event in the Capricorn Orogen: *Geological Survey of Western Australia, Record 2018/4*, 41p.
- Bodorkos, S and Wingate, MTD 2007, The contribution of geochronology to GSWA's mapping programs: Current perspectives and future directions, in *GSWA 2007 extended abstracts: promoting the prospectivity of Western Australia: Geological Survey of Western Australia, Record 2007/2*, p. 10–11.
- Bonhomme, M, Thuizat, R, Pinault, Y, Clauer, N, Wendling, R and Winkler, R 1975, Méthode de datation potassium-argon. Appareillage et technique: Note technique de l'Institut Géologie, Université de Strasbourg, v. 3, p. 35.
- Braun, J, McQueen, H and Etheridge, M 1991, A fresh look at the Late Palaeozoic tectonic history of western-central Australia: *Exploration Geophysics*, v. 22, p. 49–54.
- Clauer, N, Zwingmann, H, Liewig, N and Wendling, R 2012, Comparative  $^{40}\text{Ar}/^{39}\text{Ar}$  and K–Ar dating of illite-type clay minerals: *Earth-Science Reviews*, v. 115, p. 76–96, doi:10.1016/j.earscirev.2012.07.003.
- Cutten, HN, Johnson, SP, Thorne, AM, Wingate, MTD, Kirkland, CL, Belousova, EA, Blay, OA and Zwingmann, H 2016, Deposition, provenance, inversion history and mineralization of the Proterozoic Edmund and Collier Basins, Capricorn Orogen: *Geological Survey of Western Australia, Report 127*, 74p.
- Cutten, HNC and Johnson, SP 2018, Kuparr Tectonic Event (KU): WA Geology Online, Explanatory Notes extract: Geological Survey of Western Australia, <www.dmirs.wa.gov.au/ens>.
- Dunlap, WJ and Tessier, C 1995, Paleozoic deformation and isotopic disturbance in the southeastern Arunta Block, central Australia: *Precambrian Research*, v. 71, p. 229–250.
- Duvall, AR, Clark, MK, van der Pluijm, BA and Chuanyou, L 2011, Direct dating of Eocene reverse faulting in northeastern Tibet using Ar-dating of fault clays and low-temperature thermochronometry: *Earth and Planetary Science Letters*, v. 304, p. 520–526.
- Gradstein, FM, Ogg, JG, Smith, AG, Bleeker, W and Lourens, LJ 2004, A new Geologic Time Scale, with special reference to Precambrian and Neogene: *Episodes*, v. 27, p. 83–100.
- Grathooff, GH and Moore, DM 1996, Illite polytype quantification using WILDFIRE© calculate X-ray diffraction patterns, v. 44, no. 6, p. 835–842.
- Haines, PW, Hand, M and Sandiford, M 2001, Palaeozoic synorogenic sedimentation in central and northern Australia: A review of distribution and timing with implications for the evolution of intracontinental margins: *Australian Journal of Earth Sciences*, v. 48, p. 911–928.
- Heinrichs, H and Hermann, AG 1990, *Praktikum der analytischen Geochemie*: Springer-Verlag, Berlin, Germany, 669p.
- Hess, JC and Lippolt, HJ 1994, Compilation of K–Ar measurements on HD-B1 standard biotite, in *Phanerozoic time scale edited by GS Odin: IUGS Subcommittee on Geochronology, Paris, Bulletin of Liaison and Information of the International Union of Geological Sciences (IUGS) Subcommittee on Geochronology 12*, p. 19–23.
- Hetzl, R, Zwingmann, H, Mulch, A, Gessner, K, Akal, C, Hampel, A, Güngör, T, Petschick, R, Mikes, T and Wedin, F 2013, Spatiotemporal evolution of brittle normal faulting and fluid infiltration in detachment fault systems: A case study from the Menderes Massif, western Turkey: *Tectonics*, v. 32, p. 364–376.
- Howell, DA, Mitchell, CL, Howe, GA, Evans, DM, Ward, LA and Friedman, R 2017, The Munalu Ni sulphide deposit, southern Zambia: a multi-stage, mafic-ultramafic, magnetic sulphide-magnetite-apatite-carbonate megabreccia: *Ore Geology Reviews*, doi:10.1016/j.oregeorev.2017.02.034.
- İşik, V, Uysal, IT, Caglayan, A and Seyitoglu, G 2014, The evolution of intraplate fault systems in central Turkey: structural evidence and Ar–Ar and Rb–Sr age constraints for the Savcili Fault Zone: *Tectonics*, v. 33, p. 1875–1899, doi:10.1002/2014TC003565.
- Johnson, SP, de Waele, B, Evans, D, Banda, W, Tembo, F, Milton, JA and Tani, A 2007, Geochronology of the Zambezi supracrustal sequence, southern Zambia: A record of Neoproterozoic divergent processes along the southern margin of the Congo Craton: *The Journal of Geology*, v. 115, p. 355–374.
- Johnson, SP, Sheppard, S, Rasmussen, B, Wingate, MTD, Kirkland, CL, Muhling, JR, Fletcher, IR and Belousova, EA 2011a, Two collisions, two sutures: punctuated pre-1950 Ma assembly of the West Australian Craton during the Ophthalman and Glenburgh Orogenies: *Precambrian Research*, v. 189, no. 3–4, p. 239–262, doi:10.1016/j.precamres.2011.07.011.
- Johnson, SP, Sheppard, S, Thorne, AM, Rasmussen, B, Fletcher, IR, Wingate, MTD and Cutten, HN 2011b, The role of the 1280–1250 Ma Mutherbukin Tectonic Event in shaping the crustal architecture and mineralization history of the Capricorn Orogen, in *GSWA 2011 extended abstracts: promoting the prospectivity of Western Australia: Geological Survey of Western Australia, Record*, p. 1–3.
- Johnson, SP, Thorne, AM, Tyler, IM, Korsch, RJ, Kennett, BLN, Cutten, HN, Goodwin, J, Blay, OA, Blewett, RS, Joly, A, Dentith, MC, Aitken, ARA, Holzschuh, J, Salmon, M, Reading, A, Heinson, G, Boren, G, Ross, J, Costelloe, RD and Fomin, T 2013, Crustal architecture of the Capricorn Orogen, Western Australia and associated metallogeny: *Australian Journal of Earth Sciences*, v. 60, no. 6–7, p. 681–705, doi:10.1080/08120099.2013.826735.
- Korhonen, FJ, Johnson, SP, Fletcher, IR, Rasmussen, B, Sheppard, S, Muhling, JR, Dunkley, DJ, Wingate, MTD, Roberts, MP and Kirkland, CL 2015, Pressure–temperature–time evolution of the Mutherbukin Tectonic Event, Capricorn Orogen: *Geological Survey of Western Australia, Report 146*, 64p.
- Korhonen, FJ, Johnson, SP, Wingate, MTD, Kirkland, CL, Fletcher, IR, Dunkley, DJ, Roberts, MP, Sheppard, S, Muhling, JR and Rasmussen, B 2017, Radiogenic heating and craton-margin plate stresses as drivers for intraplate orogeny: *Journal of Metamorphic Geology*, v. 35, no. 6, p. 631–661, doi:10.1111/jmg.12249.
- Kralik, M, Clauer, N, Holnsteiner, R, Huemer, H and Kappel, F 1992, Recurrent fault activity in the Grimsel test site (GTS, Switzerland): revealed by Rb–Sr, K–Ar, and tritium isotope techniques: *Journal of the Geological Society*, v. 149, p. 293–301.

- Kübler, B 1968, Evaluation quantitative du métamorphisme par la cristallinité de l'illite: Bulletin Centre Recherche Pau-SNPA, v. 2, p. 385–397.
- Li, ZX, Bogdanova, SV, Collins, AS, Davidson, A, Waele, B de, Ernst, RE, Fitzsimons, ICW, Fuck, RA, Gladkochub, DP, Jacobs, J, Karlstrom, KE, Lu, S, Natapov, LM, Pease, V, Pisarevsky, SA, Thrane, K and Vernikovsky, V 2008, Assembly, configuration, and break-up history of Rodinia: A synthesis: *Precambrian Research*, v. 160, no. 1–2, p. 179–210, doi:10.1016/j.precamres.2007.04.021.
- Liewig, N, Clauer, N and Sommer, F 1987, Rb–Sr and K–Ar dating of clay diagenesis in Jurassic sandstone oil reservoirs, North Sea: *American Association of Petroleum Geologists Bulletin*, v. 71, p. 1467–1474.
- Lobens, S, Bense, FA, Wemmer, K, Dunkl, I, Costa, CH, Layer, P and Siegesmund, S 2011, Exhumation and uplift of the Sierras Pampeanas: preliminary implications from K–Ar fault gouge dating and low-T thermochronology in the Sierra de Comechingones (Argentina): *International Journal of Earth Sciences*, v. 100, p. 671–694.
- Lonker, SW and Gerald, J 1990, Formation of coexisting 1M and 2M polytypes in illite from an active hydrothermal system: *American Mineralogist*, v. 75, no. 11–12, p. 1282–1289.
- MacNeill, M, Marshall, N and McNamara, C 2018, New insights into a major Early–Middle Triassic rift episode in the NW Shelf of Australia, in *AEGC Extended Abstracts 2018: First Australasian Exploration Geoscience Conference*, Sydney, Australia, 18 February 2018, 5p.
- Mancktelow, N, Zwingmann, H, Campani, M, Fuegenschuh, B and Much, A 2015, Timing and conditions of brittle faulting on the Siltal-Brenner Fault Zone, Eastern Alps (Austria): *Swiss Journal of Geosciences*, v. 108, p. 305–326.
- Martin, DMcB, Sheppard, S, Thorne, AM, Farrell, TR and Groenewald, PB 2007, Proterozoic geology of the western Capricorn Orogen – a field guide: *Geological Survey of Western Australia, Record 2006/18*, 43p.
- Martin, DMcB, Sircombe, KN, Thorne, AM, Cawood, PA and Nemchin, AA 2008, Provenance history of the Bangemall Supergroup and implications for the Mesoproterozoic paleogeography of the West Australian Craton: *Precambrian Research*, v. 166, p. 93–110.
- Martin, DMcB and Thorne, AM 2004, Tectonic setting and basin evolution of the Bangemall Supergroup in the northwestern Capricorn Orogen: *Precambrian Research*, v. 128, no. 3–4, p. 385–409.
- Maxwell, DT and Hower, J 1967, High-grade diagenesis and low-grade metamorphism of illite in the Precambrian Belt Series: *American Mineralogist*, v. 52, p. 843–857.
- McDougall, I and Harrison, TM 1999, *Geochronology and thermochronology by the  $^{40}\text{Ar}/^{39}\text{Ar}$  method*: Oxford University Press, UK, 269p.
- Merriman, RJ and Frey, M 1999, Patterns of very low-grade metamorphism in metapelitic rocks, in *Low-grade metamorphism edited by M Frey and D Robinson*: Blackwell Science Ltd, Cambridge, UK, p. 61–107, doi:10.1002/9781444313345.ch3.
- Mory, AJ, Crowley, JL, Backhouse, J, Nicoll, RS, Bryan, SE, López Martínez, M and Mantle, DJ 2017, Apparent conflicting Radian–Wardian (middle Permian) CA-IDTIMS and palynology ages from the Canning Basin, Western Australia: *Australian Journal of Earth Sciences*, v. 64, no. 7, p. 889–901, doi:10.1080/08120099.2017.1365586.
- Mottram, CM, Kellett DA, Barresi, T, Zwingmann, H, Friend, M, Todd, A and Percival, JB 2020, Syncing fault rock clocks: Direct comparison of U–Pb carbonate and K–Ar illite fault dating methods: *Geology*, v. 48, no. 12, p. 1179–1183, doi:10.1130/G47778.1.
- Occhipinti, SA 2007, Neoproterozoic reworking in the Paleoproterozoic Capricorn Orogen: Evidence from  $^{40}\text{Ar}/^{39}\text{Ar}$  ages: *Geological Survey of Western Australia, Record 2007/10*, 41p.
- Odin, GS 1982, Interlaboratory standards for dating purposes, in *Numerical dating in stratigraphy, part 1 edited by G Odin*: John Wiley and Sons, Chichester, US, p. 123–148.
- Olierook, HKH, Plavska, D, Reddy, SM, Yao, W, Clark, C, Occhipinti, SA and Kylander-Clark, ARC 2019, Neoproterozoic hydrothermal activity in the West Australian Craton related to Rodinia assembly or breakup?: *Gondwana Research*, v. 68, p. 1–12, doi:10.1016/j.gr.2018.10.019.
- Pevear, DR 1999, Illite and hydrocarbon exploration: *Proceedings of the National Academy of Sciences*, v. 96, no. 7, p. 3440–3446, doi:10.1073/pnas.96.7.3440.
- Piechocka, AM, Sheppard, S, Fitzsimons, IC, Johnson, SP, Rasmussen, B and Jourdan, F 2018, Neoproterozoic  $^{40}\text{Ar}/^{39}\text{Ar}$  mica ages mark the termination of a billion years of intraplate reworking in the Capricorn Orogen, Western Australia: *Precambrian Research*, v. 310, p. 391–406, doi:10.1016/j.precamres.2018.04.006.
- Pirajno, F, Thorne, AM, Mernagh, TP, Creaser, RA, Hell, A and Cutten, H 2010, The Abra deposit: A polymetallic mineral system in the Edmund Basin, Capricorn Orogen, Western Australia, in *13th Quadrennial IAGOD Symposium Proceedings edited by NJ Cook: Giant Ore Deposits Down-Under, Adelaide, South Australia, 2010/04/06*: International Association on Genesis of Ore Deposits (IAGOD), p. 112–114.
- Pleuger, J, Mancktelow, N, Zwingmann, H and Manser, M 2012, K–Ar dating of synkinematic clay gouges from Nealpine faults of the Central, Western and Eastern Alps: *Tectonophysics*, v. 550–553, p. 1–16.
- Quentin de Gromard, R, Kirkland, CL, Howard, HM, Wingate, MTD, Jourdan, F, McInnes, BI, Danišik, M, Evans, NJ, McDonald, BJ and Smithies, RH 2019, When will it end? Long-lived intracontinental reactivation in central Australia: *Geoscience Frontiers*, v. 10, no. 1, p. 149–164, doi:10.1016/j.gsf.2018.09.003.
- Rasmussen, B, Fletcher, IR, Muhling, JR, Thorne, AM, Cutten, HN, Pirajno, F and Hell, A 2010, In situ U–Pb monazite and xenotime geochronology of the Abra polymetallic deposit and associated sedimentary and volcanic rocks, Bangemall Supergroup, Western Australia: *Geological Survey of Western Australia, Record 2010/12*, 31p.
- Reynolds, RC 1963, Potassium–rubidium ratios and polytypism in illites and microclines from the clay size fractions of Proterozoic carbonate rock: *Geochimica et Cosmochimica Acta*, v. 27, p. 1097–1112.
- Ring, U and Gerdes, A 2016, Kinematics of the Alpenrhein-Bodensee graben system in the Central Alp: Oligocene/Miocene transtension due to formation of the Western arc: *Tectonics*, v. 35, p. 1367–1391, doi:10.1002/2015TC004085.
- Roberts, NMW and Walker, RJ 2016, U–Pb geochronology of calcite-mineralized faults: Absolute timing of rift-related fault events on the northeast Atlantic margin: *Geology*, v. 44, no. 7, p. 531–534.
- Sasseville, C, Tremblay, A, Clauer, N and Liewig, N 2008, K–Ar age constraints on the evolution of polydeformed fold–thrust belts: The case of the Northern Appalachians (southern Quebec): *Journal of Geodynamics*, v. 45, p. 99–119.
- Shaw, RD, Sexton, M and Zeilinger, I 1995, The tectonic framework of the Canning Basin, WA, including 1:2 million structural elements map of the Canning Basin: *Geoscience Australia, Record 1994/48*, 89p.
- Sheppard, S, Johnson, SP, Wingate, MTD, Kirkland, CL and Pirajno, F 2010, *Explanatory Notes for the Gascoyne Province*: Geological Survey of Western Australia, 336p.
- Sheppard, S, Occhipinti, SA and Nelson, DR 2005, Intracontinental reworking in the Capricorn Orogen, Western Australia: The 1680–1620 Ma Mangaroo Orogeny: *Australian Journal of Earth Sciences*, v. 52, p. 443–460.
- Sheppard, S, Rasmussen, B, Muhling, JR, Farrell, TR and Fletcher, IR 2007, Grenvillian-aged orogenesis in the Palaeoproterozoic Gascoyne Complex, Western Australia: 1030–950 Ma reworking of the Proterozoic Capricorn Orogen: *Journal of Metamorphic Geology*, v. 25, p. 477–494.
- Solum, JG, van der Pluijm, BA and Peacor, DR 2005, Neocrystallization, fabrics and age of clay minerals from an exposure of the Moab Fault, Utah: *Journal of Structural Geology*, v. 27, p. 1563–1576.
- Srodon, J and Eberl, DD 1984, Illite, in *Micas edited by SW Bailey*: Mineralogical Society of America, *Reviews in Mineralogy*, v. 13, p. 495–544.
- Steiger, RH and Jäger, E 1977, Subcommission on geochronology: Convention on the use of decay constants in geo- and cosmochronology: *Earth and Planetary Science Letters*, v. 36, p. 359–362.

- Thébaud, N and Zwingmann, H 2012, Dating brittle deformation in the Yilgarn Craton, Western Australia, *in* AGU Fall Meeting Abstracts: American Geophysical Union, Fall Meeting, Paper No. T21A2549T.
- Torgersen, E and Viola, G 2014, Structural and temporal evolution of a reactivated brittle–ductile fault – part I: Fault architecture, strain localization mechanisms and deformation history: *Earth and Planetary Science Letters*, v. 407, p. 205–220, doi:10.1016/j.epsl.2014.09.019.
- Torgersen, E, Viola, G, Zwingmann, H and Harris, C 2015, Structural and temporal evolution of a reactivated brittle–ductile fault – part II: Timing of fault initiation and reactivation by K–Ar dating of synkinematic illite: *Earth and Planetary Science Letters*, v. 407, p. 221–233.
- Uysal, IT, Mutlu, M, Altunel, E, Karabacak, V and Golding, SD 2006, Clay mineralogical and isotopic (K–Ar,  $\delta^{18}\text{O}$ ,  $\delta\text{D}$ ) constraints on the evolution of the North Anatolian Fault Zone, Turkey: *Earth and Planetary Science Letters*, v. 243, p. 181–194.
- Uysal, IT, Piane, CD, Todd, AJ and Zwingmann, H 2020, Precambrian faulting episodes and insights into the tectonothermal history of north Australia: microstructural evidence and K–Ar,  $^{40}\text{Ar}$ – $^{39}\text{Ar}$ , and Rb–Sr dating of syntectonic illite from the intracratonic Millungera Basin: *Solid Earth*, no. 11, p. 1653–1679, doi:10.5194/se-11-1653-2020.
- van der Pluijm, BA, Hall, CM, Vrolijk, PJ, Pevear, DR and Covey, MC 2001, The dating of shallow faults in the Earth's crust: *Nature*, v. 412, p. 172–175.
- Velde, B and Hower, J 1963, Petrological significance of illite polymorphism in Paleozoic sedimentary rocks: *American Mineralogist*, v. 48, p. 1239–1254.
- Viola, G, Scheiber, T, Fredin, O, Zwingmann, H, Margreth, A and Knies, J 2016, Deconvoluting complex structural histories archived in brittle fault zones: *Nature Communications*, v. 7, no. 13448, doi:10.1038/ncomms13448.
- Viola, G, Zwingmann, H, Mattila, J and Käpyaho, A 2013, K–Ar illite age constraints on the Proterozoic formation and reactivation history of a brittle fault in Fennoscandia: *Terra Nova*, v. 25, p. 236–244.
- Warr, LN and Mählmann, RF 2015, Recommendations for Kübler Index standardization: *Clay Mineralogy*, v. 50, p. 283–286.
- Wingate, MTD 2002, Age and palaeomagnetism of dolerite sills of the Bangemall Supergroup on the Edmund 1:250 000 sheet, Western Australia: Geological Survey of Western Australia, Record 2002/4, 48p.
- Wingate, MTD and Bodorkos, S 2007, 156602: granophyric dolerite sill, No. 36 Well; Geochronology Record 695: Geological Survey of Western Australia, 5p.
- Wingate, MTD, Bodorkos, S and Sircombe, KN 2007, 148972: feldspathic sandstone, Ulna Well; Geochronology Record 689: Geological Survey of Western Australia, 7p.
- Wingate, MTD, Campbell, IH, Compston, W and Gibson, GM 1998, Ion microprobe U–Pb ages for Neoproterozoic basaltic magmatism in south-central Australia and implications for the breakup of Rodinia: *Precambrian Research*, v. 87, no. 3–4, p. 135–159, doi:10.1016/S0301-9268(97)00072-7.
- Wingate, MTD and Giddings, JW 2000, Age and palaeomagnetism of the Mundine Well dyke swarm, Western Australia: Implications for an Australia–Laurentia connection at 755 Ma: *Precambrian Research*, v. 100, p. 335–357.
- Wingate, MTD, Kirkland, CL, Blay, OA and Johnson, SP 2015, 206991: metadolerite sill, Gap Well; Geochronology Record 1263: Geological Survey of Western Australia, 4p.
- Wingate, MTD, Kirkland, CL and Cutten, HN 2012a, 143440: felsic metavolcaniclastic rock, Nicken Bore; Geochronology Record 1029: Geological Survey of Western Australia, 6p.
- Wingate, MTD, Kirkland, CL and Cutten, HN 2014, 189224: dolerite sill, Sawback Range; Geochronology Record 1211: Geological Survey of Western Australia, 4p.
- Wingate, MTD, Kirkland, CL, Cutten, HN and Thorne, AM 2012b, 143445: dolerite sill, Waldburg Homestead; Geochronology Record 1077: Geological Survey of Western Australia, 4p.
- Wingate, MTD, Kirkland, CL, Cutten, HN and Thorne, AM 2012c, 143450: dolerite sill, Top Camp Well; Geochronology Record 1079: Geological Survey of Western Australia, 4p.
- Wingate, MTD, Kirkland, CL and Johnson, SP 2013, 195826: monzogranitic gneiss, McCarthy Well; Geochronology Record 1104: Geological Survey of Western Australia, 5p.
- Wingate, MTD, Lu, Y, Cutten, HN and Johnson, SP 2018, 210006: quartzite, North West Coastal Highway; Geochronology Record 1488: Geological Survey of Western Australia, 6p.
- Wingate, MTD, Lu, Y and Cutten, HN 2019, 210047: siltstone, Ilgarari Outcamp; Geochronology Record 1641: Geological Survey of Western Australia, 5p.
- Zi, JW, Rasmussen, B, Muhling, JR, Fletcher, IR, Thorne, AM, Johnson, SP, Cutten, HN, Dunkley, DJ and Korhonen, FJ 2015, In situ U–Pb geochronology of xenotime and monazite from the Abra polymetallic deposit in the Capricorn Orogen, Australia: Dating hydrothermal mineralization and fluid flow in a long-lived crustal structure: *Precambrian Research*, v. 260, p. 91–112.
- Zwingmann, H, Mancktelow, N, Antognini, M and Lucchini, R 2010a, Dating of shallow faults: New constraints from the AlpTransit tunnel site (Switzerland): *Geology*, v. 38, p. 487–490.
- Zwingmann, H and Mancktelow, N 2004, Timing of Alpine fault gouges: *Earth and Planetary Science Letters*, v. 223, p. 415–425.
- Zwingmann, H, Offler, R, Wilson, T and Cox, S 2004, K–Ar dating of fault gouge in the northern Sydney Basin, NSW, Australia – implications for the breakup of Gondwana: *Journal of Structural Geology*, v. 26, p. 2285–2295.
- Zwingmann, H, Yamada, K and Tagami, T 2010b, Timing of brittle faulting within the Nojima fault zone, Japan: *Chemical Geology*, v. 275, p. 176–185.

The ages of fault movements on the Mount Vernon and Quartzite Well Fault systems that transect the Edmund Basin of the Capricorn Orogen have been determined using K-Ar geochronology. Isotope results for authigenic  $1M$  and  $2M_1$  illite polytypes in separated  $<0.1 \mu\text{m}$  clay fractions of lithified fault gouge define the 885–782 Ma Kuparr Tectonic Event, as well as younger, previously unrecognized faulting events in the Capricorn Orogen at 663, 346 and 238 Ma. Although K-Ar geochronology has commonly been applied elsewhere to dating Phanerozoic tectonic events, this is one of the first examples globally to apply the method to dating of Proterozoic events.



Further details of geoscience products are available from:

Information Centre  
Department of Mines, Industry Regulation and Safety  
100 Plain Street  
EAST PERTH WA 6004  
Phone: (08) 9222 3459 Email: [publications@dmirs.wa.gov.au](mailto:publications@dmirs.wa.gov.au)  
[www.dmirs.wa.gov.au/GSWApublications](http://www.dmirs.wa.gov.au/GSWApublications)